JGR Solid Earth

RESEARCH ARTICLE
10.1029/2024JB029200

Pressure Monitoring of Disposal Reservoirs in North-Central Oklahoma: Implications for Seismicity and Geostorage

B. Allen[1], K. Murray[2], P. Ogwari[1], F. Suriamin[1], J. I. Walter[1], and N. W. Hayman[1]

[1]Oklahoma Geological Survey, Norman, OK, USA, [2]Murray GeoConsulting, LLC, Denver, CO, USA

Key Points:

- The fluid pressure in the Arbuckle Group of North-Central Oklahoma is decreasing from 2016 to 2020
- Dynamic responses to stress fluctuations from solid earth tides and seismic waves vary significantly between different measuring wells
- There is a first order phase change in the pressure injection relationship above which nearby injection has a weaker effect on pressure

Supporting Information:

Supporting Information may be found in the online version of this article.

Correspondence to:

B. Allen,
benjamin.m.allen-1@ou.edu

Citation:

Allen, B., Murray, K., Ogwari, P., Suriamin, F., Walter, J. I., & Hayman, N. W. (2024). Pressure monitoring of disposal reservoirs in North-Central Oklahoma: Implications for seismicity and geostorage. *Journal of Geophysical Research: Solid Earth*, *129*, e2024JB029200. https://doi.org/10.1029/2024JB029200

Received 27 MAR 2024
Accepted 6 OCT 2024

Author Contributions:

Conceptualization: K. Murray
Data curation: B. Allen
Formal analysis: B. Allen, P. Ogwari, F. Suriamin, J. I. Walter, N. W. Hayman
Funding acquisition: K. Murray
Investigation: K. Murray, P. Ogwari, F. Suriamin, J. I. Walter
Methodology: B. Allen, K. Murray
Project administration: N. W. Hayman
Resources: K. Murray
Supervision: N. W. Hayman
Writing – original draft: B. Allen, J. I. Walter, N. W. Hayman
Writing – review & editing: B. Allen, P. Ogwari, F. Suriamin, J. I. Walter, N. W. Hayman

Abstract Disposal of industrial wastewater and activities such as CO_2 underground sequestration depend upon pressure conditions within deep geologic reservoirs. Sometimes, injection and storage are associated with induced seismicity, suggested to result from reservoir compartmentalization, leakage into faults, or other mechanisms in the subsurface. To understand subsurface pressure conditions within a major regional disposal reservoir, the Arbuckle Group of Oklahoma, we monitored the water levels in 15 inactive injection wells. The wells were monitored at 30-s intervals, with eight wells monitored since September 2016, and an additional seven from July 2017. All the wells were monitored until early March 2020. Since 2016, hydraulic head decreased in 13 of the 15 wells, proportional to near-borehole fluid pressure even considering decreasing regional injection volumes during this period. The well pressures respond to three types of perturbations: (i) gravitational fluctuations (a.k.a. solid-earth tides) (ii) distal and proximal earthquakes, and (iii) injections into nearby wells. Parameterization of tidal responses illustrates that the near wellbore environments have negative fluid flux (i.e., are leaking). Earthquakes cause differing pressure responses from well to well, with some highly sensitive to proximal events, some to distal events, and some apparently insensitive. Injections have variable impacts in some cases masking tidal and earthquake pressure signals. Collectively, there appears to be a threshold injection rate above which well pressure becomes less sensitive to the volume of injections within 15 km. Multi-scale geological structure and temporal permeability changes are likely controlling the pressure field, indicating leakage of fluids across the system.

Plain Language Summary A common industry practice is to inject fluids that are produced during oil and gas extraction back into the ground. However, movement and exchange of the fluids in the subsurface can be difficult to monitor, and wastewater injection has led to an increase in earthquakes, also known as induced seismicity. Understanding the flow of these fluids is potentially instructive for geological sequestration of carbon-dioxide to reduce greenhouse gas emissions, and subsurface storage of cleaner-burning fuels such as hydrogen. Here, we highlight how pressure monitoring in wells shows how complex the subsurface is, with varying pressure changes over space and time. Moreover, the pressures responded to earthquakes and gravitational shifts from the orbits of the sun and moon which allow for temporal analysis. We investigate these changes in an attempt to better understand flow in the Arbuckle Group, a deep disposal reservoir associated with induced seismicity in the mid-continental United States.

1. Introduction

Disposal of waste fluids into deep geologic reservoirs, such as salt-water disposal (SWD) by the oil and gas industry, is a standard practice (e.g., Engle et al., 2014). A key knowledge gap surrounding SWD concerns the scale of flow across subsurface reservoirs and the poroelastic pressure response of the formation to injection. On the one hand, case studies suggest that disposal reservoirs are highly compartmentalized, potentially by faults, with sharp gradients in pressure changes and subsurface flow (Guglielmi et al., 2021; Ortiz et al., 2019). Alternatively, correspondence between underground injection and reactivation of seismogenic faults appears to occur over broader, regional scales (Dempsey et al., 2014; Ge et al., 2022; Hsieh & Bredehoeft, 1981; Skoumal et al., 2020). Even in reservoirs known to undergo pressure fluctuations and induced seismicity, containment of the reservoir by geologic seals remains difficult to assess over a wide range of spatial and temporal scales (White et al., 2014). As safe disposal zones are increasingly viewed as a storage resource for CO_2 and for other fluids (Lemons et al., 2019; Middleton et al., 2020; Schultz et al., 2023), there needs to be further progress in understanding reservoir capacity in a heterogeneous subsurface.

In order to further investigate the subsurface mechanics of SWD, we require insight into the underlying stress conditions. At present several competing models have been suggested. These models make a Mohr-Coulomb geomechanics stability criteria which reduces the normal attractive stress, promoting fault slip. More specifically they suggest various pathways for this effect, including pressure builds up in compartmentalized reservoirs (Keranen & Weingarten, 2018), poroelastic stress disturbance of inherited intraplate tectonics structures (Barbour et al., 2017; Goebel et al., 2017), and fluid filling and pressurizing faults (Barbour, 2015; Ortiz et al., 2019).

Hydrogeologic parameters and conditions control the reservoir response to the injected fluids at depth. For example, relatively impermeable faults can lead to compartmentalization of the injection reservoir (Keranen et al., 2013; Smye et al., 2024). Alternatively, faults and surrounding damage zones may be more permeable than reservoir and underlying basement rocks and provide a pathway for enhanced fluid flow (Pollyea et al., 2019). The degree to which vertical fluid flow occurs, as well as the significance of fault-sealed pressure gradients, remains uncertain, as does the relative roles of proximal (i.e., <5 km) versus distal pressure changes (i.e., > 10 km) that may bring faults close to failure (Goebel et al., 2017; Walsh & Zoback, 2015; Yeck et al., 2016). Induced earthquakes from SWD operations are often described as the result of fluid pressure fluctuations that drive critically stressed faults closer to their failure threshold (Roeloffs, 1996). A recent example from the Delaware basin of New Mexico/Texas indicated that local hydrogeologically heterogeneous conditions may cause large fluid-pressure fluctuations and/or faults are weaker than typically modeled (Smye et al., 2024).

Here, we aim to better understand the behavior of disposed fluids and fluid pressures in a storage reservoir, the Arbuckle Group in Oklahoma. At present, Oklahoma subsurface conditions are mostly described by oil and gas industry public data from well drilling that were not necessarily collected to test these hypothesis. We report on a multiyear well-pressure monitoring program conducted by the Oklahoma Geological Survey (OGS) utilizing inactive Arbuckle disposal wells examining temporal perturbations from 30 s to days as well as the long term trend. While these data have already provided some insight into the poroelastic properties of the Arbuckle in response to the 2016 Pawnee and Cushing earthquakes (Kroll et al., 2017), the full data set has not yet been analyzed for spatial or temporal changes or reservoir response. The data greatly expand the spatial footprint of well-pressure monitoring relative to a single USGS monitored well in Osage County of northeast Oklahoma (Barbour & Beeler, 2021; Barbour et al., 2017, 2019). The present study covers the 3.5 years after the peak of both seismic activity and wastewater injection into the Arbuckle in 2015 (Walter et al., 2020). A well in Kansas has also provided data historically, but its monitoring period ended approximately when this project began (Ansari et al., 2019). The network we report on here comprises 15 wells across the area that was affected by elevated induced seismicity in the mid-2010s (Langenbruch & Zoback, 2016; Walsh & Zoback, 2015).

This study was designed for a better view of the spatial pressure distribution over a large area prone to induced seismicity. The study area includes 14 wells that vary between 3.5 and 200 km apart shown in Figure 1. Previous studies of some of these wells and similar wells worldwide tend to focus on near-wellbore effects of single wells (Barbour, 2015; Hsieh et al., 1988; Liao et al., 2020). Our approach instead examines the overall behavior of spatially distributed wells. We investigate the regional heterogeneity of Arbuckle hydrogeology, general trends in its storage capacity over time, and the sensitivity of the hydrogeology to short-duration dynamic strain changes from passing seismic waves, tidal forces, and ongoing injection.

2. Regional Setting

This study focuses on 15 wells in north-central and northeast Oklahoma (Figure 1; Table 1). The focus of the study, the Arbuckle Group, is a Cambrian-Ordovician carbonate section regionally equivalent to the Ellenburger Group to the south, and the Knox Group to the east (e.g., Kerans, 1988). The focus area encompasses the tectonic provinces of the Cherokee Platform and the Anadarko Shelf (Northcutt & Campbell, 1995). These two predominantly Pennsylvanian-age (ca. 300 Ma) provinces are separated by the north-south trending Nemaha uplift which is identifiable by surface topographic features, including small (5–8 km) fault blocks and antithetic faults along the main trace (Lawson & Luza, 1995). The provinces broadly correlate with distinct distributions of organic thermal maturity and are related to the development of the deep Anadarko and Arkoma basins to the southwest and southeast portions of the state, respectively (e.g., Cardott, 2012). The Arbuckle is thinnest (<500 m thick) in the northeast part of the state and thickens (~2 km) and deepens toward the southwest Anadarko Basin (Figure 1) dropping from 500 m deep to greater than 8 km below the surface in the Anadarko Basin. Regionally, the Arbuckle is overlain by the porous Simpson Group, a sandstone and carbonate group also utilized across the

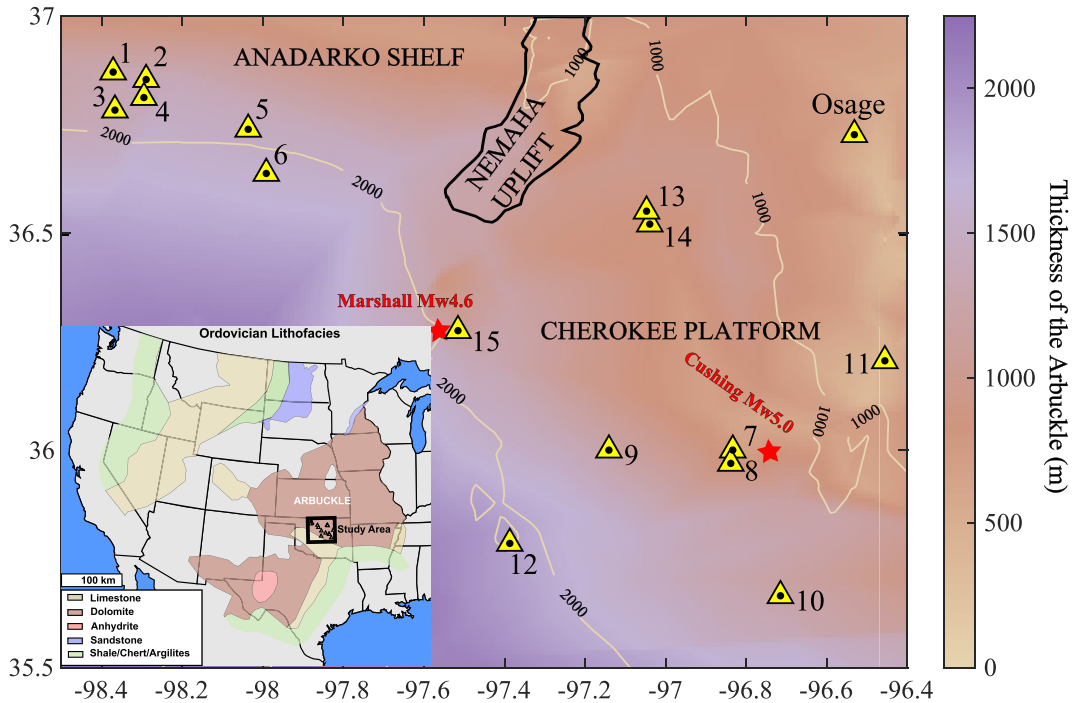

Figure 1. Contour depth map of the Arbuckle top within the study area with the contours denoting 1,000 and 2,000 m below the surface, with the Arbuckle thickness denoted by color taken from Crain and Chang (2018) and well completion logs archived by the state regulatory agency. The broad geological provinces are outlined in black and monitoring wells (triangles) are notated by number referred to within this study. Two earthquakes mentioned in this paper are denoted on the map as red stars. Inset: Extent of the Arbuckle Group carbonates, the focus of this study; map adapted from Ross (1976), The black box shows the study area within the Arbuckle Group in Oklahoma with 15 pressure monitoring wells. Note: The Arbuckle depths in the map are relatively imprecise relative to the individual well records reported here.

Table 1
A List of the Wells Monitored in This Study Along With Their Fluid Levels and the Dates They Were Instrumented

Well	API	County	Well name	Date instrumented	Initial fluid depth (meters)	Average fluid change (cm/month)
1	3500323106	Alfalfa	Clark W SWD 2811 2-27	8/1/2016	97.84	−44.76
2	3500322737	Alfalfa	Diamondback SWD 2710 2-5	8/1/2016	113.69	−0.10
3	3500323033	Alfalfa	Tatum Rose SWD 2710 1-5	8/1/2016	118.57	−46.34
4	3500322247	Alfalfa	Presley 2–27 SWD	8/1/2016	21.34	−38.07
5	3505322987	Grant	Harley SWD 2-11	8/2/2016	121.62	−23.63
6	3505322487	Grant	K9 SWDW1	8/2/2016	54.25	35.29
7	3511923946	Payne	Ethridge 25-3 SWD	8/12/2016	19.90	−57.28
8	3511923926	Payne	Wilson 11-1 SWD	8/12/2016	24.38	−74.75
9	3511923642	Payne	Bostian 1–25 SWD	9/28/2016	62.18	−24.99
10	3508123802	Lincoln	Many Drinks 1 SWD	12/9/2016	46.94	−38.53
11	3511723617	Pawnee	School Land 2-16	12/9/2016	110.95	1,086.50
12	3508324032	Logan	Harvey 1–11 SWD	9/28/2016	127.41	−49.56
13	3510324285	Noble	Mat SWD 1-36	2/8/2017	73.88	−8.63
14	3510324350	Noble	Superman 1–13 SWD	2/8/2017	116.13	−5.99
15	3504724818	Garfield	Olmstead 21-21N-3W 1 SWD	6/22/2017	154.84	−21.60

Note. Well 11 shows a large increase due to operations during the monitoring period and is not used in this study.

state as an injection target (Suhm, 2016). Overlying these rocks are several shale units, including the Devonian Woodford shale (e.g., Al-Shaieb et al., 1994), whose relatively low permeability acts as a hydrogeologic seal.

While some Arbuckle wells produce hydrocarbons (Rottman, 2018), there are few quantitative constraints on its reservoir properties compared to shallower units that have recent hydrocarbon exploration. A borehole synthesis found large variations with matrix porosity varying from <1% in calcite-rich matrices to >7% in dolomitic matrices, though vuggy sections could have whole-rock porosities as high as 18% (Rottmann, 2018). Additionally, large-scale variations in porosity, ranging from breccias resolvable in core to karst-collapse facies, are resolvable in regional studies and near-surface studies in correlative units such as the Ellenburger of Texas (Al-Shaieb & Lynch, 1993; Loucks et al., 2004). The Arbuckle in Oklahoma is found to exhibit orders-of-magnitude variations in primary and secondary permeability; for example, hand-held air permeameter measurements of core permeabilities range from <1 mD (9.87e−16 m^2) for most matrix-rich cross-bedding flow, to >200 mD (1.98e−13 m^2) for more porous along-bedding and fracture flow (Morgan & Murray, 2015). Geologic controls on the permeability and specific storage of fluid in both Kansas and Oklahoma are multifaceted and largely inferred from borehole geophysical logging (Franseen, 2000; Franseen & Byrnes, 2012; Franseen et al., 2004). Controls on porosity include faults, dolomitization, thermal maturity controls on gas phases, variable sealing units above the Arbuckle, and/or a variable burial history leading to over-compaction in many areas (Davies, 1979; Rottmann, 2018; G. Wang et al., 2015).

Two previous efforts investigated the hydrogeologic response with direct sub-hourly pressure measurements of the Arbuckle near our study area. In an investigation of the USGS-monitored Osage County well, Burbank DDD 1, the pressure response to solid earth tide pressure variations suggested that there is a volumetric vertical flux of fluid, "leaky" flow into the measured wellbore system (Barbour et al., 2019). The Osage well has been the subject of several studies examining the response of the borehole pressures to several of the same stimuli that we will be examining in this paper (Barbour & Beeler, 2021; Barbour et al., 2019; C.-Y. Wang et al., 2018). These studies showed a stable to slightly increasing fluid pressure over time. Additionally, the well responses of two of the earliest installed wells of this study in the Southern Cherokee Platform (Wells 7, 8 on Figure 1) suggest that the hydrogeology of the Arbuckle is altered in response to adjacent coseismic shaking, such as the 2016 5.8 Pawnee and 5.0 Cushing earthquakes (Kroll et al., 2017), potentially with the enhanced permeability facilitated by active karstic fractures (Barbour & Beeler, 2021; Elkhoury et al., 2006).

Important insights into seismicity and pressure variations in the Arbuckle also can be drawn from studies in the Wellington Field, Kansas (Ansari et al., 2019). These Kansas measurements unfortunately ended when all 15 of our monitoring wells came online. The monitored Kansas well, KGS 1–28, does show a similar trend to the Osage USGS well with slightly increasing pressure over time. Aside from those site-specific well studies, in Southern Kansas there are a large number of wells that are subject to quarterly reservoir pressure tests and with publicly reported values. There, Arbuckle permeability variations are apparently widespread and closely related to pressure variations in wells, many of which are under-pressured compared to the overlying stratigraphy and hydrostatic pressure (Holubnyak et al., 2018).

In this paper we examine the overall fluid pressure measured from the Arbuckle over 3.5 years in relation to the fluid injection, shown in blue in Figure 2a. Within the longer term trends, there are shorter transients from pressure fluctuations from seismic waves, as well as fluid response to the orbital gravitational changes. Previous studies (Ansari et al., 2019; Barbour, 2015; Barbour et al., 2017; Langenbruch & Zoback, 2016; Langenbruch et al., 2018) predict increasing fluid pressure in the Arbuckle with time and continued injection, potentially reactivated basement faults, which produced greater than 2000 M>2.5 earthquakes in the area during monitoring. As explained below, we do not find any evidence of increasing pressure at both local and regional scales.

3. Methods

This study summarizes over 3-year of field data collection that entailed extensive use of state regulatory records, coordination with oil-and-gas well operators, and many different types of static and dynamic data. All of the collected well pressure data and several additional data and metadata are available as an OGS open-file report (Murray et al., 2024b). Shut-in wells without recent SWD activity or nearby seismicity were chosen through a search of regulatory records and access provided by operators. All of the wells report the time of shut-in as greater than 2 months prior to the instrumentation (Table S2 in Supporting Information S1). Wells 1 and 10 have no

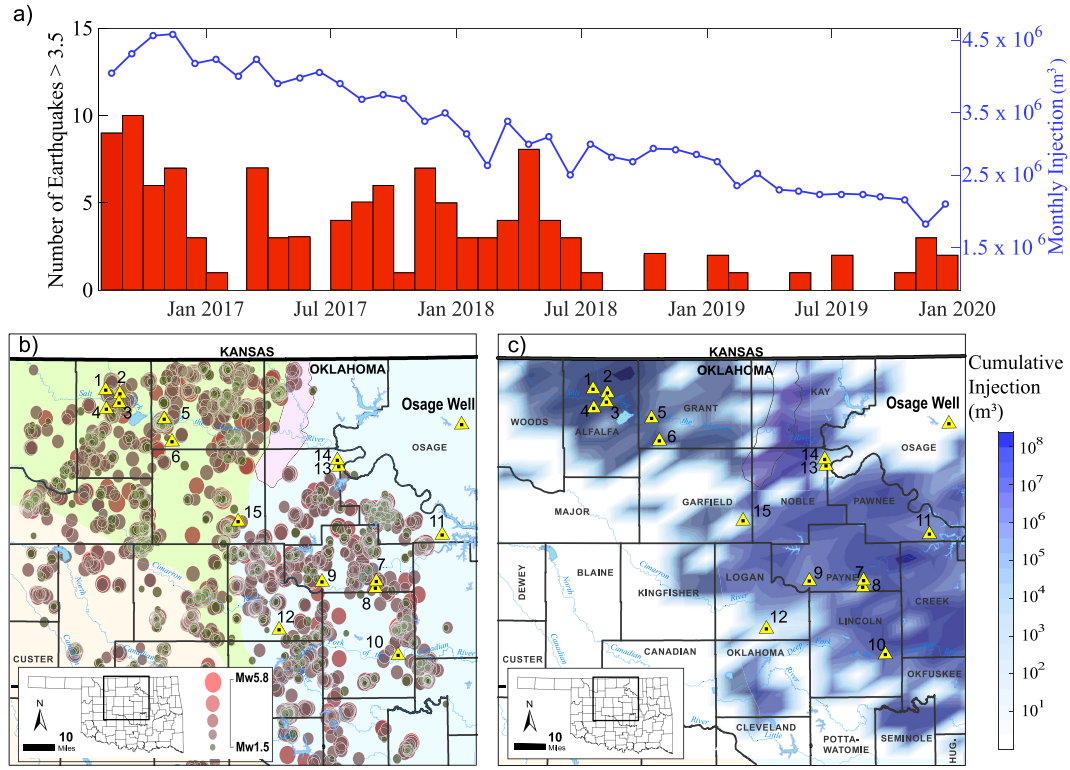

Figure 2. (a) The number of earthquakes M > 3.5 and the amount of salt-water disposal into the Arbuckle. (b) Map showing the earthquakes during the monitoring period. (c) Map showing the cumulative injected volume over the monitoring interval with a grid size of 1.75 km^2 and linear interpolation between grid squares for smoothing. The Osage monitoring well is monitored by the USGS and reported in Barbour et al. (2017), and some of the injection into the Arbuckle in Osage County is not readily available.

records of injection since 2013, the first year of available full state injection reporting. Initial interfaces and fluid density column were read and recorded before a data cable was threaded through the wellbore and seal cap, and pressure and temperature sensors were lowered approximately 23 m below the liquid-air interface. The Solinst Leveloggers recorded the pressure and temperature at 30 s intervals with an uncertainty of $\pm 0.05^{o}$ C and ± 0.05 kPa. Various field problems (i.e., such as lowering the Leveloggers as the fluid levels fell much more than expected) were addressed during monthly site visits to download the data (Figure S1 in Supporting Information S1).

An initial eight wells were instrumented in August 2016, and seven more wells were instrumented over the next year to broaden the geographic profile. The well-sensor deployment shown in Figure 1 was designed to monitor large injection volumes in Alfalfa County and another large-injection site at the edge of Creek and Payne County; both areas have local injections that are an order of magnitude higher than the rest of the state during the study period. Additional wells were instrumented through late 2016–2017 near epicenters of earthquakes M > 4.

The monitoring wells were distributed across the area of interest with wells 1–4 being within 10.4 km of each other and two pairs of "partner" wells, 7 & 8, and wells 13 & 14 are both 3.4 km apart. The wells were monitored until early 2020 and the data are supplemented with regulatory records which record daily injection rates into nearby active SWD wells. Daily injection volumes are required to be reported for Class II (Enviromental Protection Agency designation for enhanced recovery, fluid disposal and hydrocarbon storage) wells permitted for injection into Arbuckle Group within an area of interest in North-Central Oklahoma (Murray et al., 2023). Well 11 is not included in this study due to poor records stemming from nearby operational activities.

The Levelogger pressures were converted to fluid levels by the fluid density; this fluid head will be discussed throughout the paper as the well level and/or pressure head. The pressure was then proportional to the bottom-hole pressure due to the weight of the fluid column, calculated with $P_{bore} = \int_{bottom}^{top} \rho_f g \, dz$ where the fluid density ρ_f is integrated over the fluid column to get the bottom-hole pressure, and g is the gravitational acceleration. We ignore

friction terms in our calculations assuming that the fluid changes happen slowly enough that we can treat the pipe walls as a no-slip boundary. Initial static and fluid density columns are taken from the OGS open-file report (Murray et al., 2024b). The short temporal pressure perturbations are then found by applying a low-pass filter with a temporal cutoff of less than 6 hr, and down-selecting for pressures twice the average fortnight pressure. The fluid levels were analyzed using models of tidal forces, combined with linear poroelastic theory, and assessments of pressure perturbations from injections and earthquakes across the 14 wells.

Previous researchers have also used gravitational tidal strains (Ackworth et al., 2015; Gao et al., 2020; Hvorslev, 1951; Merritt, 2004), also known as "earth tides," as a means of inspecting the hydrogeological properties of the surrounding aquifer; this technique has been specifically applied to the Arbuckle in Oklahoma using the Osage well (Barbour et al., 2019; C.-Y. Wang et al., 2018) resolving the M2 tidal signature and Wells 7 and 8 with the initial year of data (Kroll et al., 2017). This analytical approach assumes a uniform pore strain due to the cyclic earth tides, and uses the wellbore fluid response to estimate the flow into the system assuming the permeability and porosity of the reservoir (Barbour et al., 2019; C.-Y. Wang et al., 2018). The methods used in C.-Y. Wang et al. (2018) are expanded by Gao et al. (2020) to further include wellbore damage (increased permeability or reduction).

It should be noted that many of the monitored wells were previously chemically and/or mechanically permeability-enhanced to allow for faster throughput of fluid. Wells 12, 14 and 15 are open-hole completions with no permeability enhancement reported, but all the other wells have some form of permeability enhancement. Wells 7, 8 and 10 received fracking and HCl treatments, while the other wells are all chemically treated with HCl, or in the case of the older wells 6 and 9, the acid used is NE/FE acid. For this reason, when examining the wellbore response and attempting a physical parameterization of the Arbuckle reservoir we will use the more complete derivation of Gao et al. (2020) which includes terms for wellbore permeability being different than the host rock, which is described by the skin coefficient (Hawkins, 1956).

In order to compare to previous studies and extract parameters describing the wellbore system, we examine the tidal response in the well levels. The predicted volumetric strain from the earth tides was calculated using the *earthtide* R package (Kennel & Parker, 2023) which is based on the original Fortran package Eterna 3.40 (Hartmann & Wenzel, 1995) with updated calculations (Kurdyavtsev, 2004). The fluid tidal cycles were determined as well records, using a filtered Fourier transform for the daily and semi-daily cycles using SLUGTide (Allègre et al., 2016; Xue et al., 2013).

The change in pressure far away from any perturbations ($r \rightarrow \infty$) due to the gravitational earth tides can be written

$$P_{gi} = A_i B K_r \cos(\omega_i t + \Phi_i) \tag{1}$$

where A_i is the amplitude of the gravitational stress, ω_i is the frequency, and Φ_i is the phase of the ith tidal component. B is the Skempton's coefficient, and K_r is the bulk modulus of the surrounding rock matrix. In this study we have taken the bulk matrix as a constant, but acknowledge that it could vary locally and will vary depending on the pore pressure. This whole approach assumes uniform properties, and the bulk matrix could change by a few percent. The resulting well pressure is therefore calculated at the wellbore given the assumptions that the flow around an individual well can be assumed to be uniform and non-divergent, the rock is homogeneous linear poroelastic material, and that the permeability and porosity are not significantly changed by the poroelastic stresses of the earth tide. This approach assumes that variation in nearby injection shown in Figures 3 and 4 is spatially and temporally independent of the earthtide response, and instead allows a steady state flux into and out of the modeled wellbore system.

The expected phases and amplitudes can be estimated using the parameters in Table 2 to solve the Navier equation (Gao et al., 2020) varying the variables within the bounds set in Table 2; the variables are the seven values at the bottom of the table, and the eight values above are treated as constants. The permeability and porosity bounds are taken from core and well log measurements of the Arbuckle (Morgan & Murray, 2015). Skempton's coefficient B varies between 0 and 1 by definition, but the other variables are unknown parameters. The wellbore storage C is the amount of fluid of the wellbore system, which is usually measured empirically. The skin coefficient s denotes the difference in the wellbore permeability to the host rock (Hawkins, 1956). A negative skin coefficient

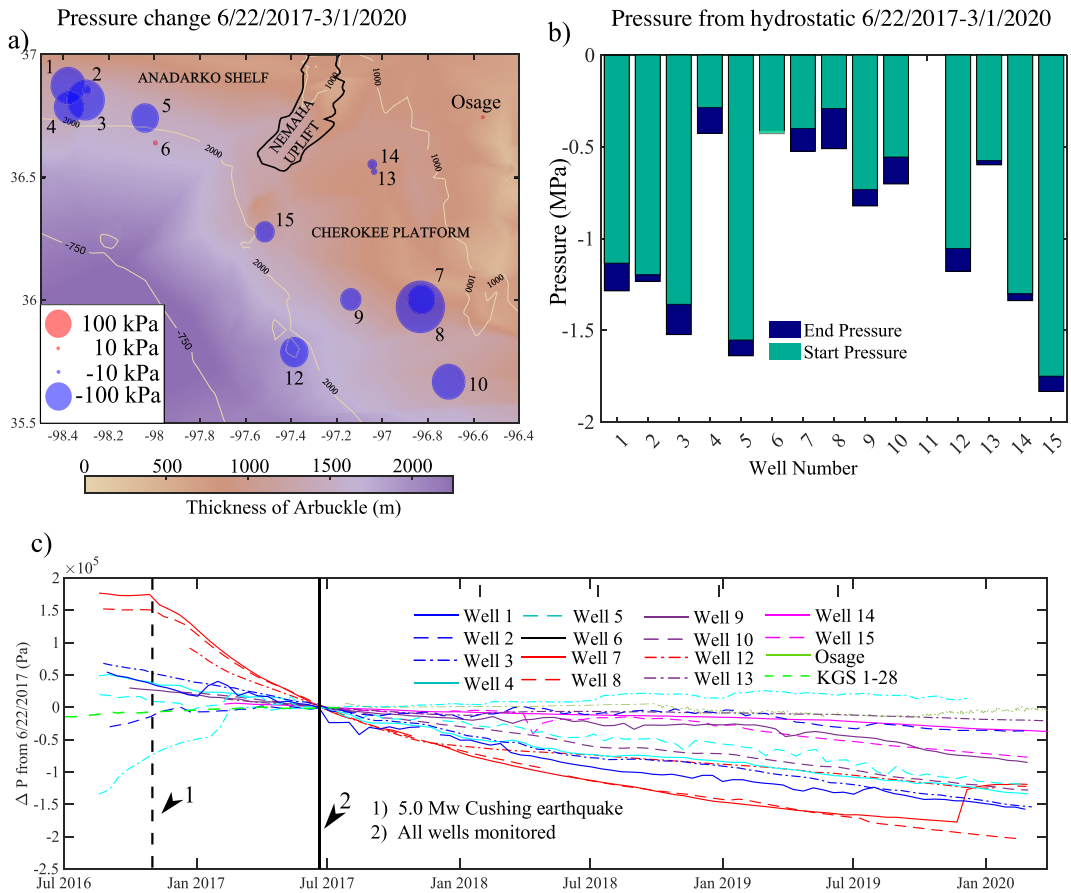

Figure 3. (a) The total pressure change during the monitoring period starting from 6/22/2017 to 3/01/2020. Well 6 and Osage are the only wells showing a steadily increasing trend. (b) The beginning and ending pressure of each well from 6/22/2017 to 3/01/2020 in reference to the hydrostatic pressure from the top of the borehole. (c) All fluid elevations averaged over 2-week intervals and normalized to the initial monitoring date of the last implemented monitoring well (Well 15). Well 7 & 8 show a drastic change in fluid head following the Cushing earthquake on 11/06/2016 denoted by line 1. Line 2 denotes when all wells went online and is the comparison zero point for all the pressures changes.

represents enhanced permeability around the wellbore system compared to the host rock and a positive skin represents reduced permeability. The equation has seven unknowns, and with the amplitude and phase of both the M2 and O1 tide, there are four variables.

As taken from Gao et al. (2020), with the inclusion of f allowing for a positive or negative volumetric flux into or out of the wellbore system, the equation for a semi-confined aquifer with a damage zone around the wellbore is given by:

$$\nabla^2 P - H' P = \frac{\phi \mu c_t}{k}\left(\frac{\partial P}{\partial t} - \frac{\partial B K_r \epsilon_V}{\partial t}\right) \tag{2}$$

where ϕ is the porosity, μ is the viscosity, $c_t = \left(\frac{1}{K_r} + \phi \frac{1}{K_f}\right)$ is the compressibility of the system, which is the sum of the inverse of the bulk moduli of fluid and rock phases. $H' = K'/(b' T_r)$ is the anisotropy coefficient determined by the ratio of the conductivity K' with the aquitard parameters denoted with a prime. T_r is the horizontal transmissivity of the aquifer, and b' is the thickness of the aquitard. The sign of f denotes the direction of the fluid flux into (+) or out of (−) the reservoir. This coefficient determines the percentage of flow that travels vertically out of the system across the aquitard compared with the horizontal flow. The flow in the reservoir is denoted with:

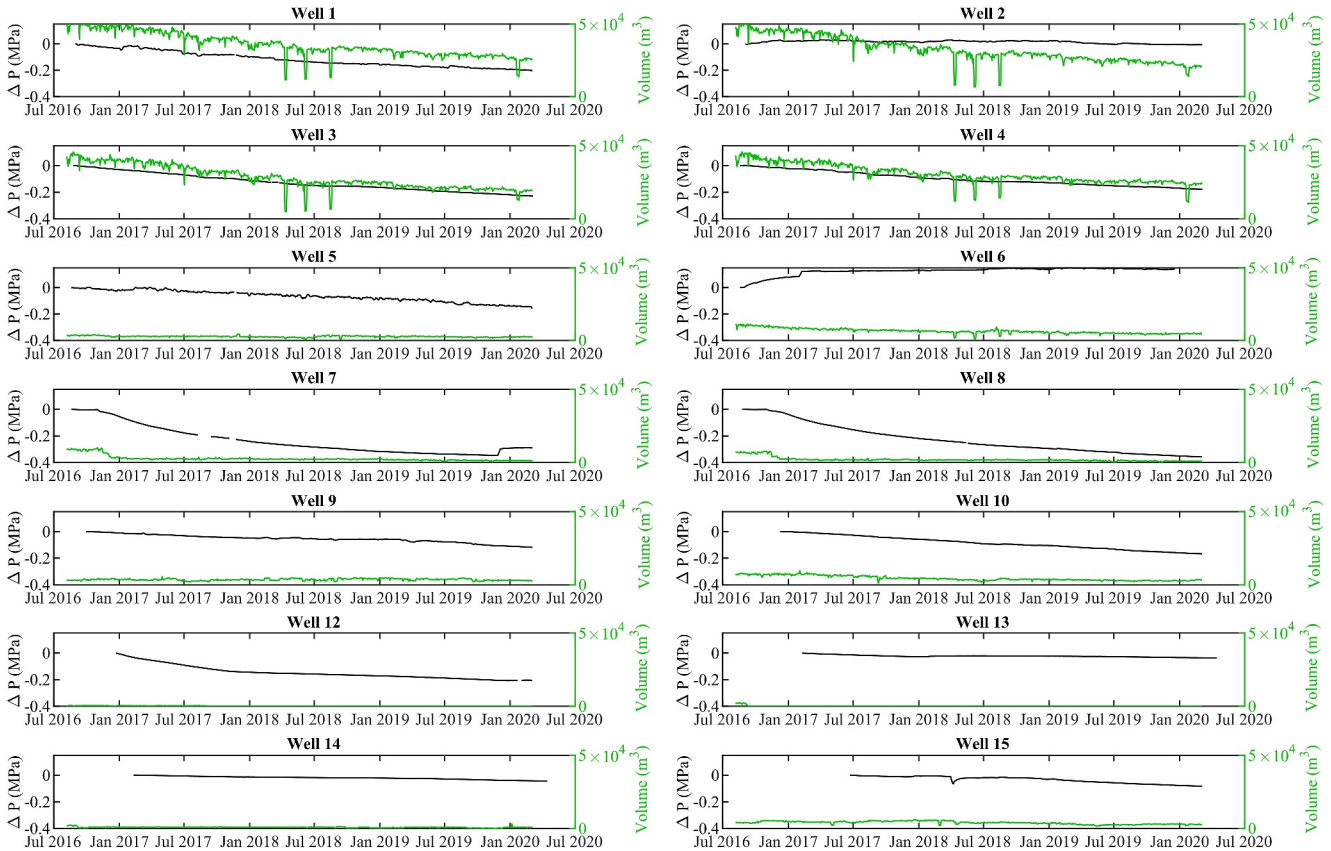

Figure 4. The fluid elevation in the monitoring wells discussed in this report in black and the injected volume within 15 km in green. Wells 1–4 in Alfalfa County have the most injection by an order of magnitude. Wells 7–8 have the largest pressure drop over the monitoring period. Pressure change is calculated from the beginning of monitoring for each individual well.

$$\beta = \sqrt{fH' + \frac{\omega i \mu c_t}{k}} \tag{3}$$

where ω_i is the frequency of the ith tidal signature and the other variables are denoted in Table 2. Solving for the pressure P for each tidal constituent provides a complex exponential with K_0 and K_1 being modified Bessel functions of the first and second kind respectively:

$$P_{w0}(i) = \left[1 + \frac{\omega i \mu C}{2\pi k h r_w \beta} \frac{K_0(r_w\beta)}{K_1(r_w\beta)} + \omega i \frac{sC\mu}{2kh}\right]^{-1} \left(\frac{\omega i \phi \mu c_t}{fkH' + \omega i \phi \mu c_t}\right) BK\epsilon_V \tag{4}$$

Here $C = 1/K_w * V$ and denotes the amount of fluid directly controlled by the wellbore using the compressibility of the fluid as well as the fluid in any connecting fractures. This is an empirical measurement taken immediately after start-up/shut-in of a well, since we do not have the results of this measurement we include it in our unknowns. The amplitude and phase shift of the pressure are then:

$$A_i = |P_{w0}(i)/(BK_r\epsilon_{Vi})| \tag{5}$$

$$\eta_i = \arg(P_{w0}(i)/(BK_r\epsilon_{Vi})) \tag{6}$$

As there are six loosely bounded unknowns and a non-linear equation, we created a parameter search, varying each unknown as denoted below the line in Table 3 individually over the range specified. ϕ and B were varied linearly, and the other variables were varied over a log scale. We conducted this variable search with 50 samples

Table 2
Variables Used to Solve the Poroelastic Equations

Variable		Range	Source
Well Radius	r_w	88.5–112.2 mm	OCC Form 1002 A
Casing Radius	r_c	109.5–122.2 mm	OCC Form 1002A
Aquitard Thickness	b'	200–300 m	OCC Form 1002A
Thickness of Aquifer	h	200–500 m	OCC Form 1002A
Fluid Density	ρ_f	1,000–1,200 kg/m^3	Downhole Measurements
Viscosity	μ	0.001 Pa s	Water
Bulk Modulus (Rock)	K_r	40 GPa	C.-Y. Wang et al. (2018)
Bulk Modulus (Fluid)	K_w	2.4 GPa	Water
Skempton's Coefficient	B	0–1	
wellbore Storage	C	$1 \times 10^{-7} - 10^{2}$ m^3/Pa	
Skin Coefficient	s	(−7)–7	
Anisotropy Coefficient	f	−1 or 1	Positive or negative flux
Aquitard Vertical Flow	H'_z	0–10 m^{-2}	
Permeability	k	0.1–1,000 mD	Morgan and Murray (2015)
Pore Space	ϕ	0.05–0.15	Morgan and Murray (2015)

Note. Variables in the first section are taken as given, and variables below the line are varied over the range shown denoting the assumed uncertainties.

for each unknown variable, other than $f = [1, -1]$. To reduce the solution space, we matched the resulting answers to within 10% of the M2 and O1 phase. Zero was always included in the variation of parameters, to account for the possibility of one of the variables not being important or present.

Table 3
Table of the Mean Amplitudes and Phase Changes of the $\tau_{M2} = 12.421$ hr and $\tau_{O1} = 25.819$ hr

Well	M2 amplitude (1/m)	M2 phase (degrees)	O1 amplitude (1/m)	O1 phase (degrees)
1	1.59e−07 ± 7.753e−08	14.7 ± 40.1	8.44e−08 ± 6.87e−08	2.8 ± 2.2
2	2.43e−07 ± 1.47e − 07	9.7 ± 54.1	1.51e−07 ± 1.03e−07	2.7 ± 2.3
3	1.77e−07 ± 7.60e−09	28.2 ± 2.3	2.21e−07 ± 1.70e−08	0.2 ± 0.1
4*	1.16e−06 ± 8.65e−07	−24.8 ± 35.7	8.50e−07 ± 4.25e−07	3.8 ± 2.3
5	1.40e−08 ± 8.08e−09	40.0 ± 96.9	9.32e−09 ± 6.34e−09	3.4 ± 1.8
6*	4.96e−07 ± 3.67e−07	0.7 ± 32.4	3.41e−07 ± 3.45e−07	2.6 ± 2.6
7*	2.55e−07 ± 1.57e−07	16.8 ± 12.2	2.69e−07 ± 3.05e−07	0.52 ± 1.2
8*	3.58e−07 ± 1.70e−07	16.9 ± 15.3	3.64e−07 ± 1.06e−07	1.6 ± 2.5
9	1.24e−07 ± 3.15e−08	30.5 ± 1.6	1.60e−07 ± 9.37e−08	0.4 ± 0.5
10	3.24e−07 ± 1.92e−08	15.3 ± 2.6	3.14e−07 ± 4.49e−08	0.6 ± 1.5
11	1.96e−08 ± 2.10e−08	22.2 ± 84.1	6.24e−09 ± 6.94–09	2.7 ± 1.9
12	2.31e−07 ± 3.54e−08	30.0 ± 7.5	2.75e−07 ± 3.81e−08	0.3 ± 0.5
13*	1.75e−07 ± 4.95e−08	31.14 ± 9.5	2.36e−07 ± 4.38e−08	0.4 ± 0.5
14	2.00e−07 ± 3.05e−09	33.4 ± 0.4	2.37e−07 ± 6.55e−09	0.3 ± 0.04
15	1.35e−07 ± 3.55e−08	29.2 ± 12.0	1.35e−07 ± 1.77e−07	0.2 ± 0.3

Note. A negative shows lag, and a positive shows lead. It should be noted that the tidal signatures with high variance come from wells with high nearby injection and some of the tidal signatures with moderate variance change with time marked with a *. Other examples can be found as Figures S3–S17 in Supporting Information S1.

4. Results

4.1. Long-Term Pressure Changes

At the start of the pressure monitoring all of the instrumented wells were below hydrostatic pressure, some drawing a slight vacuum upon unsealing of the wellhead. Following the unsealing of the monitoring wells, the fluid levels continued to decrease in all but one well over the course of the 3.5 years monitoring period (Figure 3c) in contrast to the slight rising pressures reported previously in the Kansas Wellington project (Ansari et al., 2019) and the continuous data from the Burbank DDD 1 well in Osage County (Barbour & Beeler, 2021; Barbour et al., 2017, 2019). For most wells, the pressure rate changes depending on the amount of injection within the nearby area and is negative across the majority of the wells regardless of whether there is recorded previous injection in the monitoring wells. We detail those observations and discuss further, considering the analysis below.

For most wells that exhibit decreasing pressures, the long term temporal pressure change has a linear correlation coefficient of $R < -0.96$ on the monthly/year scale with the change in fluid levels averaging -30 ± 15 cm/month (Table 1). There is a geographic variation to the pressure decrease as seen in Figure 3a. Of the wells not considered in the average, Well 2 shows a strong influence of near-by well injections and rises initially staying relatively stable before decreasing slightly as seen in Figure 3c. This is in contrast to Wells 1, 2, 4 which are all within 10 km of Well 2. Additionally, there are two wells that show a different trend primarily due to the 6 November 2016, M5.0 Cushing earthquake (Wells 7, 8). The only well that did not undergo pressure decreases was Well 6. Note that Well 6 does exhibit an increasing trend, similar to those found in Osage (Barbour et al., 2017) and KGS 1–28 (Ansari et al., 2019). Well 6 failed a mechanical integrity test (MIT), in which the casing/annulus is raised to the maximum injection pressure and the pressure is observed for 1–2 hr. A failure occurs if the casing does not hold pressure, suggesting a leak in the casing. The failure of the MIT in Well 6 suggests that there is a leak in the well casing, and as such not necessarily representative of the pressure of the Arbuckle possibly being contaminated by higher strata.

Two days after the M5.0 Cushing earthquake, the state-mandated closure of wells within 9.66 km (6 miles) and reduction of 25% of the last 30 days average volume (Oklahoma Corporation Commission, 2016). Additionally, wells within 24.14 km (15 miles) were not allowed to exceed the last 30 days average volume. The state regulatory agency routinely would take mitigating action to shut in wells adjacent to M4.0 or greater earthquakes and those actions led to a concomitant decrease in aftershock efficiency (Goebel et al., 2019). Fluid levels dropped by 1 m in Wells 7 and 8 following the 6 November 2016 Cushing earthquake, denoted by 1 in Figure 3c, followed by long-term fluid decrease. This pressure change corresponds with the earthquake to within the temporal resolution of our measurements (30 s) and begins several days before the injection was reduced in the immediate area. Wells 7 and 8 are 2.9 and 3.9 km away from the epicenter respectively, and injection reduced throughout the area around these wells decreased in response to the M5.0 Cushing earthquake which is shown in Figure 1. Both wells then show a decline with an exponential drop in pressure for the next 3 years. Similarly, Well 15 shows a fluid drop of over 6 m in 2 min after a M4.6 earthquake near Marshall, OK, which was 1.6 km from the monitoring well. But unlike in Wells 7 and 8, the fluid level in Well 15 increased back to pre-earthquake levels over the next three to four months before resuming the original decreasing trend.

4.2. Injection Response

As shown in Figure 2a, the monitoring period saw a decrease in total injection volumes relative to previous years. However, there was still a 2.5×10^6 m^3 monthly injection rate throughout the 3.5 years monitoring period. To explore this further, in Figure 4 we illustrate each of the well pressure changes are related to the respective proximal (within 15-km) injection from operator records of daily injection into the Arbuckle submitted to the regulatory agency, the Oklahoma Corporation Commission. There is an order of magnitude more injection around the wells in Alfalfa County (Wells 1–4) than the rest of the monitoring area as can be seen by Figure 4, matched only with one other high injection site at between Payne and Creek County. The higher injection corresponds with a much greater drop in fluid height in Wells 1, 3 and 4 compared to the pressure decrease in wells that have little to no injection within 15 km. Additionally, the influence of nearby injection can be seen in the response in Wells 1, 2 and 5 compared to the other wells even after smoothing for a daily average; raw plots can be seen in Figures S3, S4, and S7 in Supporting Information S1. These three monitoring wells (1, 2, and 5) have injectors within 100 m.

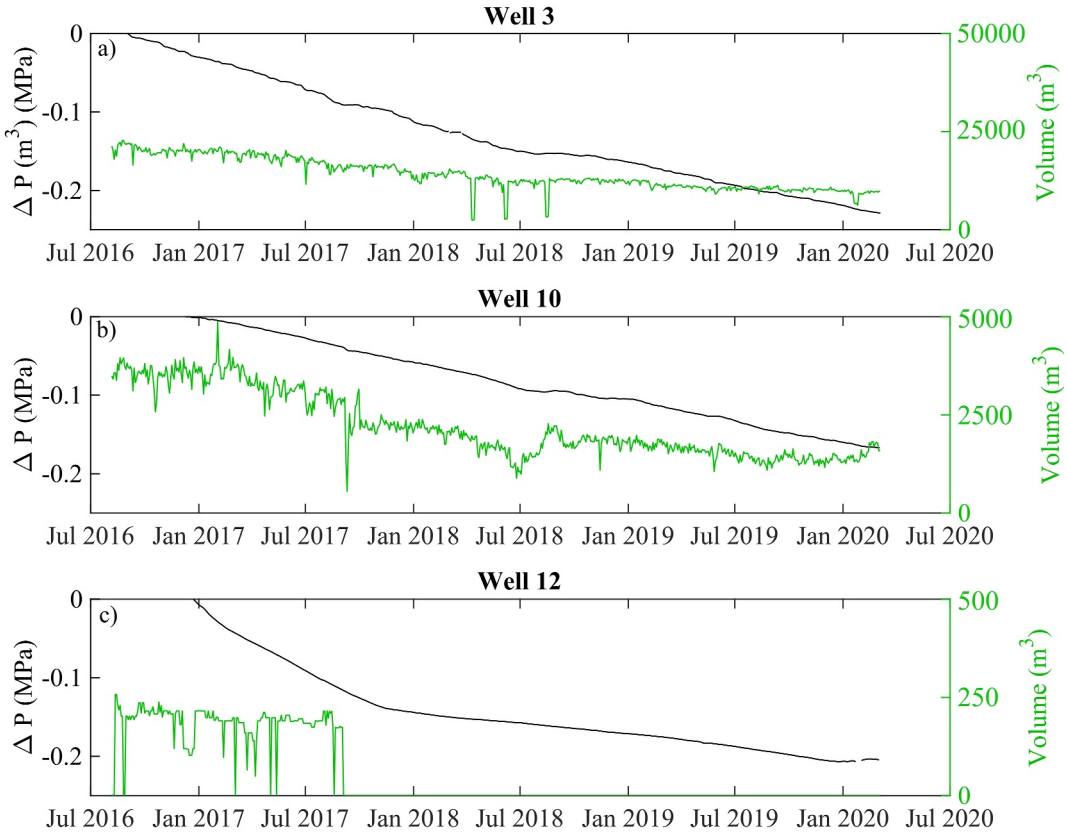

Figure 5. Plots of three of the well levels in black as well as the injection within 15 km at decreasing orders of magnitude in green (a) Well 3 with a full scale of 50,000/m^3 day (b) Well 10 with a full scale of 5,000 m^3/day (c) Well 12 with a full scale of 500 m^3/day. Additionally, Well 12 has no proximal injection for most of the monitoring period. Pressure change is calculated from the beginning of monitoring for each individual well and all show a similar change in pressure.

In several instances, we observe abrupt (e.g., Wells 2, 6, 7, 15) and gradual (e.g., Wells 3, 9, 12, 13, 14) changes in the rate of pressure decrease. These pressure-rate changes correspond with changes in injection rate and/or earthquakes. This transition to a more sensitive wellbore pressures to injected volume correspond to cessation of injection (e.g. Wells 7, 8) due to regulatory directives or other operator-specific decisions following earthquakes.

When we compare injection and pressure changes, there appears to be a transition wherein the stress changes slowly at rates of less than 1 Pa per m^3 when the injection is high within a 15 km radius. When the injection is reduced below the threshold the pressure response becomes more sensitive to injection with a rate ~10 Pa per m^3 injected within a 15 km radius (Figure 5). Additionally, there appears to be a further drop in the pressure rate change after injection in the area is reduced completely. This behavior is best represented in Well 12, due to almost all injection stopping in the area (Figure 5c). This second order phase transition between pressure and injection is also shown by wells crossing an "injection threshold" wherein pressure and nearby injection correlate, but with different pressure responses above and below a certain injection volume (Figure 6a). Additionally, there are a few wells where the changes in pressure are completely uncorrelated with injection within 15 km, but still exhibit similar declining pressure. A very strong response to injection, in a nearby injection well (<100 m) with 20 m fluid level changes, occurs in Well 5 on the time scale of 10 min that overwrites all other signatures. Well 6 shows a negative trend between change in pressure and injection within 15 km.

Probing the injection-pressure relationship a little further, Figure 6a shows a rise in the pressure rate corresponding to increased daily injection with a transition at around 1.8×10^4 m^3 of fluid injected within 15 km of Well 7. In this instance the pressure is only slightly elevated at the higher injection rates. The inset in Figure 6a shows the injection versus time, and the pressure rate threshold is found from higher injection to lower injection. A few of the wells show this transition as seen by the black and green markers in Figure 6b at approximately the

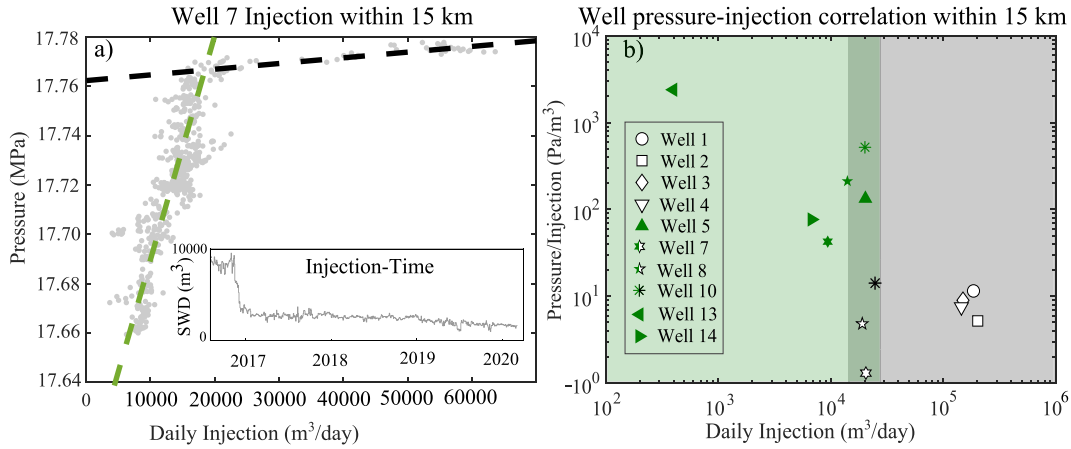

Figure 6. (a) Daily bottom-hole pressure versus injected volume per day within 15 km of Well 7. Inset illustrates that injection was relatively steady after an initial drop in 2017. (b) The rate of change of pressure in relation to injection within 15 km. Green symbols denote the greater slope seen at lower injection rates and black symbols describe the linear fit to the second flow phase seen at higher injection rates. Three wells show the transition shown in panel (a) and thus have both green and black symbols. This transition is indicated by the intersection of the green line and black line as shown in panel (a). A clear injection rate threshold is seen just below 2×10^4 m^3/day injection rate. Note that Wells 5, 9, 11, and 13 did not exhibit correlations.

same transition injection rate. The lower the injection rate into the wells within 15 km, the more influence the injection has on the pressure.

4.3. Earthquake Response

A common perturbation to fluid levels of the monitoring wells are signals from proximal and distal earthquakes. For example, the M5.0 Cushing OK earthquake severely changed the fluid pressure response of Well 7 and 8 due to coseismic poroelastic stress as documented in Kroll et al. (2017), as well as by severely altering the pore pressure conditions as indicated by dashed line-1 in Figure 3c. More distant earthquakes commonly trigger a fluid-pressure response that can be used to constrain poroelastic or hydrogeologic parameters (Elkhoury et al., 2006; Liao et al., 2020), such as was done for the Osage County well (Barbour & Beeler, 2021; Barbour et al., 2019). However, recording the induced strain from distant earthquakes requires sampling higher frequencies than our sampling rate of 30 s, which is insufficient for fitting waveforms. Despite the sample-rate limitation, observed earthquakes are identifiable as perturbations against the longer term background signal of the fluid response.

In order to study the perturbations due to earthquakes, which show up as sudden increases and decreases in the fluid levels of the wells. We use a simple automatic threshold filtering to find perturbations greater than twice the mean fluctuation in the non-gravitational response of the monitored wells. With this filter, perturbations from local earthquakes on the order of M4.0 or greater can be identified in some wells but not others. Similarly, the teleseismic signals from other larger earthquakes show a response in some wells and not others (Figure 7). The earthquakes we observed are tabulated in Tables S3 and S4 in Supporting Information S1. While local earthquakes could possibly be missed due to the sampling time, larger earthquakes, as shown in Figure 7, cause poroelastic stress changes that occur over several minutes at $P > 100$ Pa, yet still do not cause pressure changes in some of the wells. Most notably wells 7 and 8, which are 1.8 km apart and are close to identical in borehole geometry, fluid densities, and permeability enhancement, show very different responses to the teleseismic signal; Well 8 shows a clear perturbation and Well 7 shows none.

Additionally, from the number of earthquakes detected there are some wells that seem to show a stronger response to teleseismic waves, but are weakly sensitive to local events, while others show the opposite. However, there are also some earthquake events that show up in all the wells with a large enough perturbation, although the level of the pressure perturbation does change between wells (i.e., M7.9 Pentiopa de don Luis, Mexico on 02/16/2018 17:49 CDT (local time)).

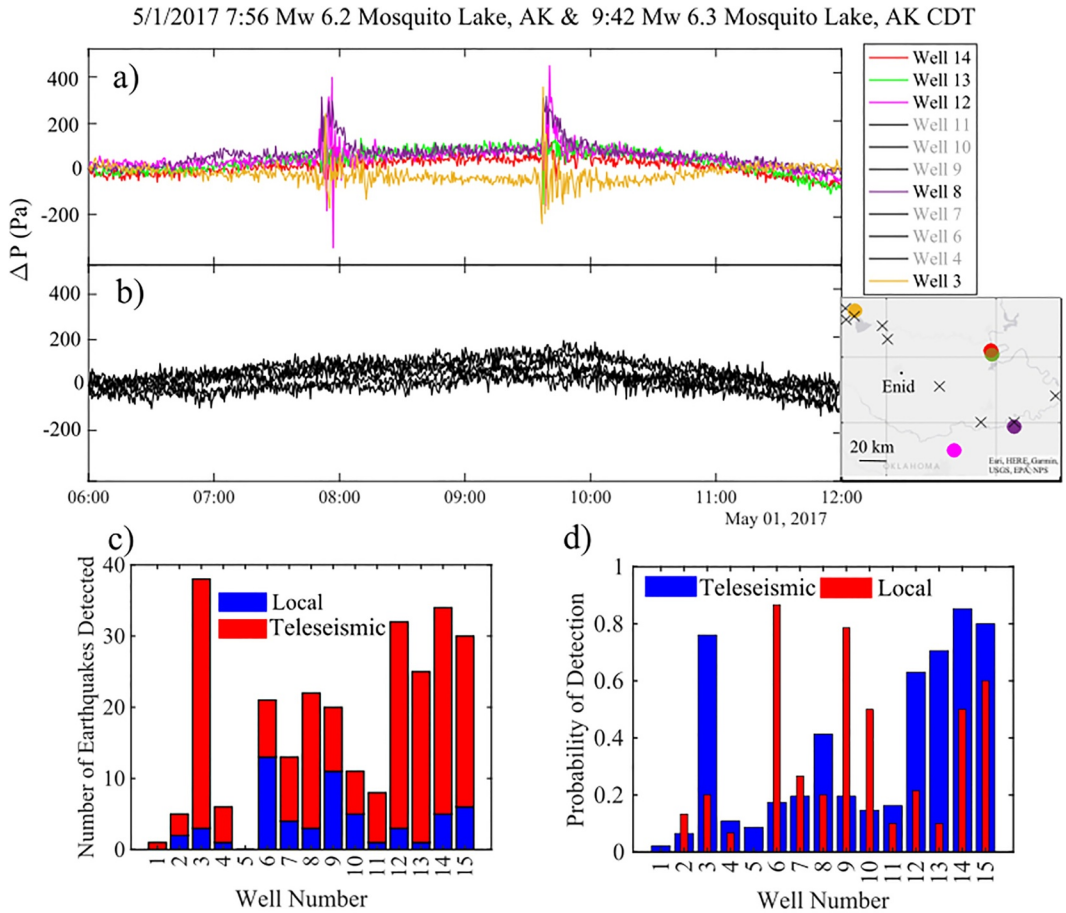

Figure 7. Earthquake signature of paired earthquakes of 6.2 and 6.3 M respectively from Mosquito Lake, AK. (a) Wells which show a signature after detrending. (b) Wells that do not show a signature after detrending. Side inset shows the locations of the wells recording the earthquake as dots, and ones that do not as '×'. (c) Sensitivity of the Arbuckle wells to detecting local seismic and global tele-seismic signatures. (d) The probabilities normalized by all events detected are shown. The earthquakes in panels (c) and (d) are automatically detected signatures with acceleration of over 2 standard deviations from the background data signature.

In summary, the mixed response of the borehole fluid pressure to seismic waves is best explained by very different local hydrological conditions. Additionally, some of the wells seem more sensitive to teleseismic waves (low frequency) compared to local smaller earthquakes (high frequency). Note that these wells were drilled into the same formation, and with similar permeability treatments. Therefore, bulk material properties cannot be the main explanation for the different teleseismic responses.

4.4. Tidal Response

Following the methods described in Gao et al. (2020), we sought to characterize the response pore stress to the solid earth-tide. Perturbations to the longer term earth-tide pressure fluctuations include the aforementioned seismic and injection responses, each of which highlights different hydrogeological and poroelastic responses between wells. While some of the wells show signals of a large range of short duration events and are not useful in the present tidal analysis, some of the wells primarily exhibit the well tides. Different wells in this study appear to exhibit differences in both hydrogeology (long-term pressure changes across a broad area) as well as poroelastic properties (short-time-scale and near-wellbore differences in strain responses).

There are three classes of earth-tide response measured in the wells: (a) overwritten/non-existent, (b) a phase change between fluid response and gravitational potential, and (c) temporal changes in phase. The first class of wells are overcome by noise, perturbed so much by short term pressure changes or with such a variable response

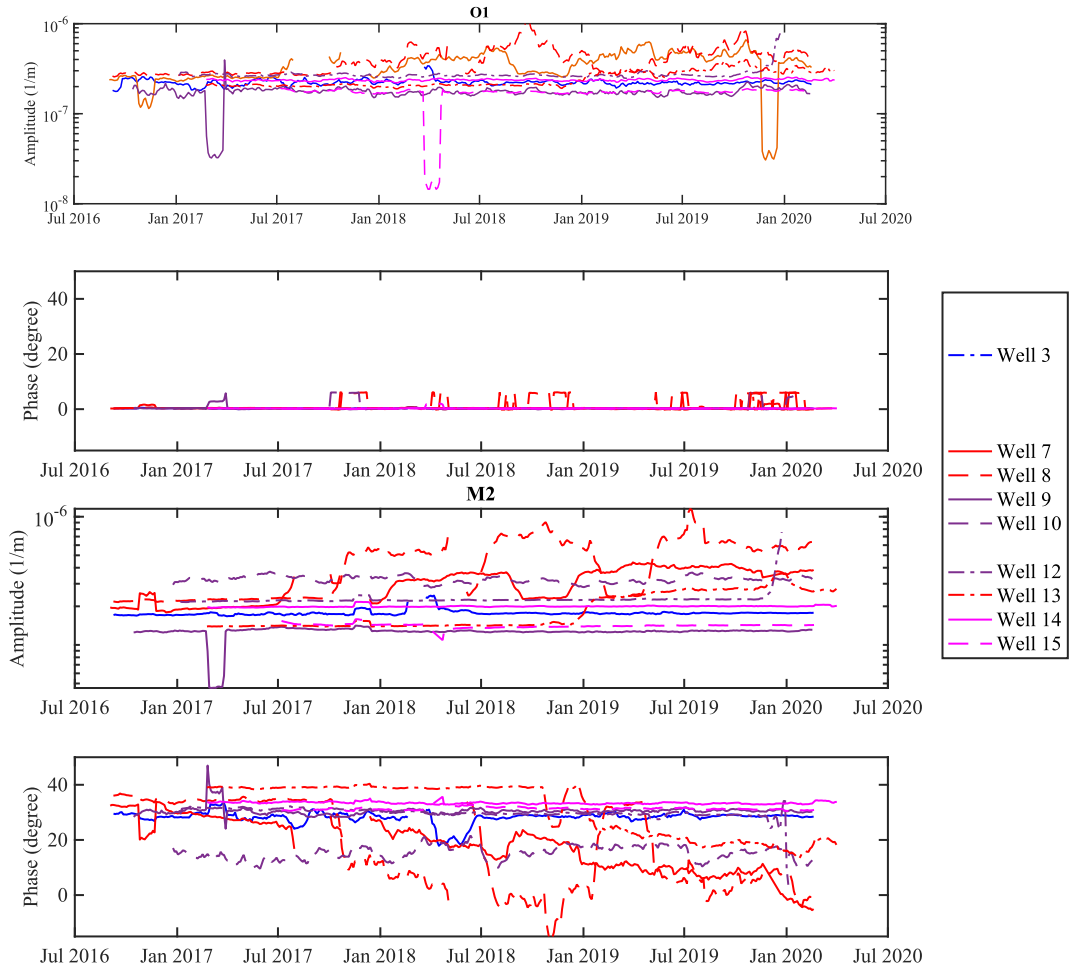

Figure 8. The tidal signatures of the wells allowing for meaningful recovery of the M2 and O1 earth tides in the fluid levels. Wells 1,2,4, 5,6 have been removed from the plot due to the noise and uncertainty. Further individual plots can be found in Supporting Information S1. (a) Amplitude of the O1 tide. (b) Phase of the O1 tide in the well levels. (c) Amplitude of the M2 tidal signature over time (d) Phase change of the M2 phase over time. Most of the wells show a phase precedence of about 40^o for the wells without significant change. This corresponds to a peak response of the fluid little over an hour before the maximal earth strain. Wells 4, 6, 7 and 8 and 13 show a change of phase over time.

to the earth tide, that no clear earth tide signature can be established. These include Wells 1, 2, 4, 5, and 6 as can be seen from the standard deviation in Table 3. The rest of the wells are shown in Figure 8. Wells 3, 9, 10, 12, 14, and 15 show a stable baseline phase change between the fluid response and the gravitational potential. Additionally, while these show a relatively constant phase and amplitude, occasionally there will be a temporal variation which will then return to the baseline. Finally, Wells 7, 8, and 13 show long-term temporal changes, starting similar to the other wells but deviating in 2017, with a rise in the amplitude and corresponding decrease in the phase over a time scale of years seen in red in Figure 8 or Figures S4–16 in Supporting Information S1.

In this study we examine the M2 and O1 tides as they are the least affected by daily barometric effects and possible interference from daily or twice daily injection operations. The most prominent tidal signature is the semidiurnal $\tau_{M2} = 12.421$ hour tide. The M2 tide has a significant temporal shift in the tidal well signal, arriving significantly $\sim 30^o$ (about an hour) before the peak compression of the earth in the area for the majority of the wells, preceding the gravitational tidal potential. In contrast, the $\tau_{O1} = 25.819$ hour period gravitational fluctuation has almost no temporal shift with the fluid-level response. Interestingly, in all but one well there is a precedence (positive phase) in the expected phase of the fluid response to the gravitational tide, although about half the wells show a large variation in the phase due to poor fitting of the tidal components, likely caused by interference from proximal injection. For some unknown reason Well 3 appears to have little perturbation

Table 4
A List of the Best Fit Parameters at the Start of the Well Monitoring, While Giving Equal Weight to the Percentage Error of η and A, of Equations 4 and 5

Well	ϕ	k(mD)	fH_z(m^2)	s	C(m^3/Pa)	B	η_{M2}	η_{O1}	A_{M2} (m^{-1})	A_{O1} (m^{-1})
1	–	–	–	–	–	–	–	–	–	–
2	–	–	–	–	–	–	–	–	–	–
3	0.02	46	−3.89e−05	−1.6	4.92e−04	0.41	28.3	0.2	1.85e−07	2.10e−07
4	–	–	–	–	–	–	–	–	–	–
5	–	–	–	–	–	–	–	–	–	–
6	–	–	–	–	–	–	–	–	–	–
7*	0.11	16	−8.89e−05	−1.4	4.64e−05	0.08	32.4	0.3	2.10e−07	2.49e−07
8*	0.14	46	−1.34e−04	−0.6	7.90e−04	0.23	35.9	0.4	2.07e−07	2.57e−07
9	0.12	0.27	−2.89e−02	−0.1	7.44e−05	0.26	30.4	0.4	1.37e−07	1.60e−07
10	–	–	–	–	–	–	–	–	–	–
12	0.01	0.28	−2.42e−03	−1.7	1.60e−07	0.44	30.0	0.3	2.27e−07	2.62e−07
13*	0.14	6.0	−7.02e−04	−4.0	1.80e−05	0.10	39.0	0.5	1.54e−07	1.99e−07
14	0.02	359	−3.26e−06	−3.2	2.03e−03	0.28	33.0	0.3	1.91e−07	2.28e−07
15	0.14	0.10	−1.00e−01	−3.7	6.61e−07	0.26	29.0	0.2	1.23e−07	1.41e−07

Note. Wells without entries have no solution. * denotes time dependence in the well tides, so this only applies in the first month after the well was instrumented. Plots of the full parameter search can be found in Figures S18–23 in Supporting Information S1.

allowing for good tidal fitting while the other wells (Wells 1, 2, and 4) show interference from proximal injection in the larger Alfalfa County region.

4.4.1. Parameterization Using Wellbore Response

The well-level response to tidal forces can be parameterized using Equation 4 (see Methods). Unfortunately, when the amplitudes are constrained to within 10% of their measured values, Wells 1, 2, 4, 5, 6, and 10 have no possible combinations of the variables that provide both the correct phases and amplitudes. The parameter search is shown in Figure 6 for the least varying well, Well 14, which also has limited nearby injection.

The negative skin coefficient (permeability enhancement around the wellbore) is also related to the wellbore storage coefficient which describes the volumetric change in the wellbore system compared to pressure changes. The sign of the anisotropy parameter f shows a net fluid loss from the system and the transmissivity is then determined by the fluid storage of the formation, S, which depends on the pore space. A $\eta_{M2} - \eta_{O1} > 20^o$ difference in phase between the M2 and O1 tide cannot be explained with Equation 5, unless both a negative flux and a negative skin coefficient are used. Our results, given the boundary and initial conditions to solve the homogeneous solutions, show that there has to be a negative flux $f = -1$ out of the surrounding wellbore system as well as enhanced near-wellbore permeability. Table 4 shows the best fit minimizing the percent error, if it is less than 10%, between both the phases and the amplitude, but as can be seen in Figure 9 there are a large set of possible parameters that can be approximated for the reservoir.

Half the wells cannot be described by Equation 4 resulting in no fits in Table 4. Wells 1, 2, 4, 5, and 6 are dominated with injection from nearby wells, resulting in poor fitting for the poroelastic strain of the tidal constituents and even using the mean fitting, are not described. Well 10 has no solution to Equation 4 within the bounds set. Wells 7, 8, and 13 are represented in Table 4 according to the initial tidal fitting, but as shown in red in Figure 8 the M2 amplitude and phase shift change dramatically over the study period and it is very unclear on what variable(s) would be changing to allow for full fitting.

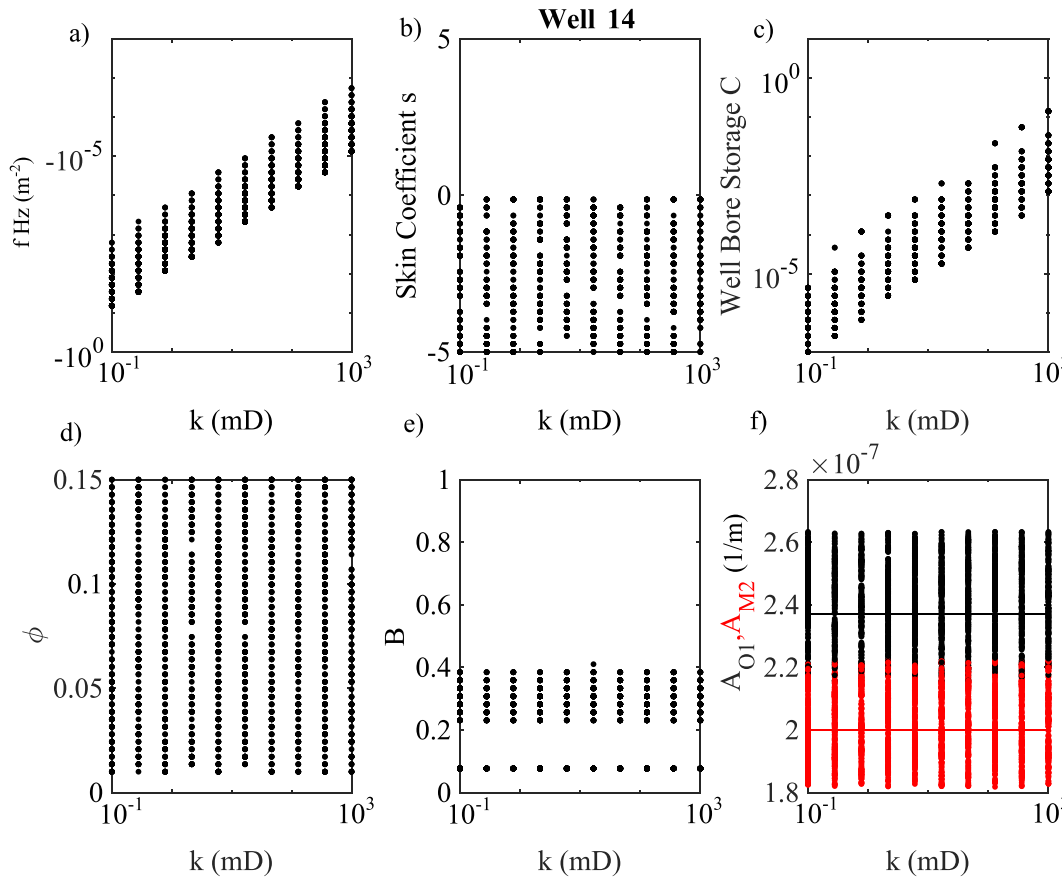

Figure 9. The allowed value of the parameters in Table 3 for the most stable well in regards to the solid earth tides. (a) Horizontal aquifer permeability k and fluid flux into the system fH'. (b) Aquifer permeability k and skin coefficient s. s is never above zero in any solution. (c) Aquifer permeability k and wellbore storage coefficient C, (d) Aquifer permeability and aquifer porosity. (e) Aquifer permeability and Skempton coefficient B. (f) Amplitudes of O1 and M2 tides. In order to get the large difference in phase observed a negative skin coefficient $s < 0$ and a negative volumetric flux are required. All permeabilities are possible, with a linear relationship to wellbore storage coefficient C and a constant order of magnitude of vertical conductivity. Further plots are available as Figures S18–23 in Supporting Information S1.

5. Discussion

There are three main results that we report on. The first, and the simplest, is that the Arbuckle is underpressured, even after large volumes of produced-water injection (3.52 km^3 from 2010) leading up to this study. The second, which is related, is that the pressure continued to drop during the monitoring period. Finally, perturbations to the pressure, such as earthquakes, tidal forces, and nearby injections, interact with the porous environment in highly heterogeneous and dynamic ways.

5.1. Finite Pressure Differences & Storage Capacity

As shown in Figure 3b the pressure in the wells is significantly below hydrostatic. Note that the study started well past the peak of seismicity and maximum SWD, and so the baseline pressure conditions are unknown. There are studies of adjacent systems such as the Hunton group (above the Arbuckle) that found pressures between 70% and 100% of hydrostatic in the Anadarko Basin, while the Woodford Shale had elevated pressures (Al-Shaieb et al., 1994). Though the baseline pressure prior to increased SWD is unknown, there are wells in our study area that have no injection history up to 7 years before this monitoring project, yet exhibit the same pressure-decreasing behavior as wells with much more recent injection. In short, the system is in an elevated state above equilibrium; that is the well levels continue to drop rather than recover toward the hydrostat.

The well pressure can vary significantly across a few kilometers as seen in Wells 4 to Wells 1–3 and Well 13 to Well 14 with pressure differences on the order of 500 kPa. Previous studies have suggested that the pressurized state resulting from earlier injections should persist for several years (Langenbruch & Zoback, 2016; Langenbruch et al., 2018). Therefore, it is somewhat counterintuitive that underpressured conditions persist even after a vast injection of fluid (3.52 km^3) since 2010. An estimate of $dP = -\frac{dV}{V}K_{rock}$ using the bulk modulus of $K_{rock} = 40$ GPa suggests that such volumes would increase the pressure in the Arbuckle up by $\delta P = 80$ MPa. Even assuming that the system includes adjacent areas where injection was somewhat lower, the pressure-change estimation would remain within an order of magnitude. Yet, the potentially large increase in pressure is not observed, with bottom-hole pressures at approximately 15 MPa from atmospheric pressure. The higher pressure estimation would only be valid if the fluid was confined within the Arbuckle, which multiple parts of this study contradict, as discussed further below. Hence, we deduce that the pressure is lower within the Arbuckle because the fluid is leaking.

5.2. Pressure Changes Over Time

Along with the static pressures, we show pressure changes over time, over the monitoring period of 3.5 years (Figure 3). In all but one well we see a declining pressure despite continuing injection. Such pressure decreases are common for short-term, near wellbore behavior in the days following an injection, but not over such wide areas and long durations. Similarly, decreasing injection over time could lead to an overall decrease in pressure of the system, potentially decreasing the hazard for induced seismicity (Langenbruch et al., 2018; Langenbruch & Zoback, 2016). In contrast we suggest that if the Arbuckle were a finite reservoir, any continued injection would continue to lead to higher regional pressure conditions (i.e., the 80 MPa change in pressure, assuming cumulative injected fluids stay within the Arbuckle Group). Note that Goebel et al. (2017) came to a parallel conclusion for the induced seismicity hazard based on earthquake statistical considerations. As an independent check on the relationship between injection history and pressure changes, we note that two of the wells have no records of injection, and yet show similar falling fluid levels as wells in the same area that were previously used for injection.

Importantly, there are examples of pressure changes that correspond directly to known examples of fluid flow away from the wellbore. For example, the failed MIT in Well 6 correlates with a large increase of fluid pressure in late 2016-early 2017. In this instance, the fluid pressure leveled off with a slight increasing trend, similar to the time period before the MIT. Well 6's behavior could stem from fluid leaking through the casing from higher pressure formations, similar to the behavior described by Barbour et al. (2019) for the Burbank DDD 1 wellbore. Note that we cannot rule out that there is some local reservoir compartmentalization leading to anomalous pressure conditions. Also note that pressures in the Arbuckle are lower than the pressures higher in the stratigraphy (Al-Shaieb & Lynch, 1993; Al-Shaieb et al., 1994), which limits possible flow upwards.

5.3. Heterogenous Pressure Responses to Earthquakes and Tidal Forces

We now turn to the heterogeneous responses to perturbations. The variable responses to distal and proximal earthquakes is one of the more intriguing observations. Inhomogeneous earthquake responses have been reported in natural gas fields and groundwater systems worldwide (King et al., 1999; Zhang & Huang, 2011). In our study, the variability in earthquake response has no apparent spatial distribution suggesting poroelastic fluid-rock interactions at scales of kilometers or less. The responses differ for proximal versus distal earthquakes as well. For example, Well 6 is more likely to respond to an Oklahoma earthquake than to an earthquake from the Pacific plate boundary, despite the larger response in other wells to the larger teleseismic earthquakes. As a general explanation for these behaviors, we describe the pore-fluid system as high- and low-pass fluid filters with differing organization of fluid storage/capacity and conductive/resistance. This filter could manifest along fractures and have a directional component due to the fracture orientation. For wells that do not respond to distal earthquakes, we suggest that a lack of response is due to large lateral transmissivity in the direction of the signal. Future work could further probe the details of this filtering mechanism.

Another perturbation to the well pressure is from cyclic waves caused by the fluctuations of the gravitational potential of the sun and moon orbiting the earth and the resulting earth strains. The pressure responses to these tidal forces also have heterogeneous expressions between wells. However, the main observation is that these pressure trends are in many cases overwritten by fluctuations caused by local injections (Wells 1, 2, 4, and 5). Yet, wells in the same area, such as Well 3, still have a dominant tidal signature despite the same nearby injections.

Wells that do have tidal signatures tend to show a precedence of the well tide relative to the earth tide. In general, such precedence is thought to result from enhanced permeability and potentially fluid flux out of the system (Barbour et al., 2017).

Theoretically, tidal strains offer the opportunity to further determine hydrogeological parameters of the reservoir (Barbour et al., 2019). To attempt this, as well as place our results in the context of the previous studies, we analyzed the tidal strains with a simplified flow model around a wellbore for each individual well (G. Wang et al., 2015). Where the model was applicable, we were able to determine that the well had a negative skin coefficient, consistent with the inferred enhanced permeability.

However, even the simplified model fails to predict and match the tidal measurements (amplitude and phase change) of over half of the wells. Some of the poor performance of the model can be attributed to the uncertainty of the measurements because of the noise of the local injection responses, or pressure effects of the local injection responses themselves. The model assumes a uniform divergence of flow into or out of the wellbore, whereas localized injections create additional sources of flow. More puzzling are the ways the well pressures mismatch the model results. For example, there is one well, Well 10, that fits the characteristic behavior shown by the other wells in this system, but cannot be described by Equation 4. Finally, some of the wells (Wells 7, 8 and 13) show a temporal variability of amplitude and phase that cannot be captured by the standard parameters we used in Table 2.

One interesting possibility is that the failure of the model to describe the tidal signature for Wells 7 and 8 is due to effects of the M5.0 Cushing earthquake. Postseismic poroelastic pressure changes have been reported worldwide (Elkhoury et al., 2006; Liao et al., 2020; Xue et al., 2013) and also in some early studies of this data set Kroll et al. (2017). Our data is temporally limited and we cannot examine long term recovery to pre-earthquake conditions.

As a method, the tidal response analysis should be taken with caution, even if it does support the hypothesis of a permeability-enhanced, leaky, and relatively sensitive system. Underlying assumptions in the model have a priori incompatibilities, such as the assumption of homogeneous fluid flow, which is inconsistent with the known fluid injection history, such as shown in Figure 2c. In practice, the poor fitting of the tidal constituents may simply be a consequence of inhomogeneity caused by injection. However, the model also fails to explain the behavior of some wells that are otherwise relatively insensitive to injection. Future successful implementation of this model will likely depend on independent measurements of wellbore and skin coefficients, as well as permeability, to reduce the set of possible solutions in Equation 4. The model will still encounter problems though as flow becomes more directional, such as around fault zones.

5.4. Pressure-Injection Relationships and Implications for Induced Seismicity

The last perturbation we consider is the acute response to injection. While a few wells show no correlation with measured pressures and injection within 15 km, most do. Three of these wells show a transition as shown in Figure 6 from being less sensitive at higher injection rates to becoming more sensitive at lower injection rates across a transition of around 2×10^4 m^3/day. The other wells fall on one side or the other of this transition. The change in pressure versus injection rate highlights a first order phase change in flow (rate of change of pressure), and potentially a pressure-dependent permeability. When the injection rate is lower than 2×10^4 m^3/day, each injected volume creates a much larger proximal (<15 km) stress change than when the injection is $>2 \times 10^4$ m^3/day.

We hypothesize that the injection-pressure threshold behavior could be related to that for induced seismicity (Langenbruch & Zoback, 2016). In detail, the suggestion of Langenbruch and Zoback (2016) and Langenbruch et al. (2018) was that injecting above 10^6 m^3/month into a 5,000 km^2 area increased the chance of M3 earthquakes or greater. This injection rate is only approximately 2X larger than that associated with the transition in the pressure–injection relationship we describe in the decreasing injection history when applied to the same scale, but there is no direct correlation between the large field falling pressures and seismicity. Additionally, our study finds that finer scale pressure variations could further complicate such inferences of induced-seismicity thresholds, given the pressure transients and sensitivity changes of wells only kilometers apart. In some ways, such a pressure-sensitive system is similar to that reported by Smye et al. (2024) for a more data-rich modeling effort on the Delaware Basin in Texas and New Mexico.

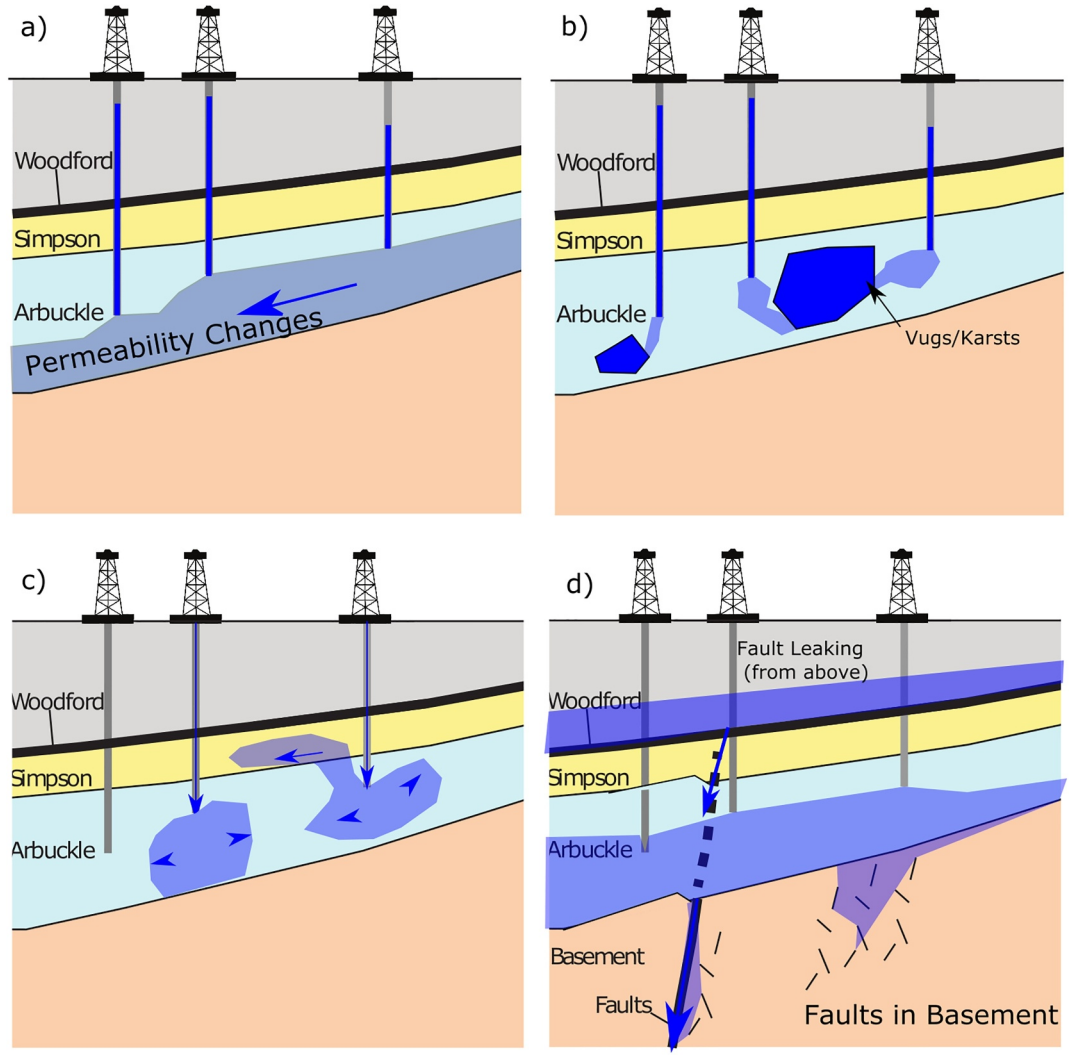

Figure 10. Conceptual illustrations (not to scale) depicting some of the possible flow structures: (a) Long scale flow showing pressure changes from spatial permeability and velocity differentials. (b) Filling up and pressurizing vacuum-sealed or gas filled vugs and pores. (c) Filling up compartments within the Arbuckle and pushing the flow to a higher permeable stratigraphy. (d) Fluid disappearing into the basement through faults, and possibility leaking from the above structure (see also Barbour et al. (2017).

5.5. Conceptual Models for Hydrogeological Controls on Pressure

Related to hypothetical injection transitions as causes of induced seismicity, one family of models envisions compartmentalized reservoirs where fluid pressure increases thereby bringing faults closer to failure (Keranen et al., 2013). Some aspects of the data, such as the fine-scale spatial heterogeneity in pressure variations could be explained by such compartmentalization. However, the broader system of leakage is, in contrast, relatively incompatible with such a conceptual model. Given the inability to quantitatively rule out the existing geological models for fluid pressure and induced seismicity, we probe four hydrogeological concepts in Figure 10: (a) fluid is traveling horizontally out of the system with permeability changes causing pressure differences due to poroelastic flow (b) fluid is filling underpressured karstic features (c) fluid is leaking into adjacent units where it flows more freely, (d) fluid is leaking through fractures and faults into the basement.

The first concept (a) of lateral flow is certainly occurring to some extent, though it places no further constraints on the finer scale heterogeneity or mixed responses to perturbations. The second concept (b) of karstic controls on pressure is appealing given that pockets of isolated fluid pressure could be accessed as fractures or other fluid pathways open up between them. We otherwise rule out this hypothesis though, because the sheer amount of fluid

injection across the region would quickly fill or equilibrate pressure differences between any macroporosity. Flow into and along the overlying formation(s), (c) is an appealing concept, but the flow would have to work against the fluid-pressure gradient. We therefore suggest that (d), flow of the dense fluids downward into basement fractures and faults, remains a good explanation for the fluid pressure regime in the Arbuckle; flow into basement faults and fractures is one of the favored previous explanations of how SWD causes seismicity (Kolawole et al., 2019). Future models that explore fracture/fault-opening and closing, variable flow rates, enabling faster flow out of the system, and even adopting rate-and-state friction models (Norbeck & Rubinstein, 2018), could help reconcile existing models and other data sets with the new insights presented here.

6. Conclusion

Well-level monitoring provides insights into fluid pressures in the deep fluid disposal formation, the Arbuckle Group carbonates, in Oklahoma from ~2017–2020. Heterogeneously changing, generally decreasing, pressures across the region, plus inhomogeneous responses to tidal forces, earthquakes, and proximal injection variation, all point to a heterogeneous, out of equilibrium hydrogeologic system. The reservoir itself is still significantly underpressured after over a decade of significant fluid injection ($>3.52 \times 10^9$ m^3), and continues to be decreasing in fluid pressure. The volume of injection and continuing falling pressures signify a leakage in the Arbuckle reservoir, an assumption here demonstrated with a model for earth-tide response. Yet, the earth-tide response model is also shown to have severe limitations when applied to a system of inhomogeneous injection and flow. The fluid-rock system also acts as a band-pass filter to passing seismic waves, causing variable fluid-pressure responses within wells to proximal and distal earthquakes. Local earthquakes also cause resolvable changes in fluid-pressure behavior, both through the subsequent decrease in injection forced by regulatory mitigation, but also through co-seismic mechanical impacts on the hydrogeology. There is also a threshold in the injection rate/volume relationship, above which the coupling between injection rate and pressure decreases. One hypothesis for the observed threshold is the overfilling of the reservoir, with flow reaching an approximately 10× more conductive unbounded stratigraphy. Alternatively, the fluid could be flowing into basement fractures and faults; flow into the basement is the standard interpretation of the fluid pressure regime favoring induced seismicity. Other hydrogeological conceptual models are not consistent with the observations. Previous models for induced seismicity infer a threshold in injection that is somewhat higher than that observed here if such a threshold promotes fault slip. Furthermore, previous studies suggest that the Arbuckle reservoir has a fixed storage capacity, with some models describing fault-compartmentalized permeability. This study in contrast illustrates ongoing leakage and renewed storage capacity, with fine-scale pressure heterogeneity from geological mechanisms, potentially opening and closing of basement faults and fractures.

Data Availability Statement

The well data (initial well completions, density column measurements and pressure monitoring files) in this manuscript are published as Murray et al. (2024b) and can be found on Zenodo (Murray et al., 2024a) as a HDF5 dataset (Koranne, 2011). The USGS DDD 1 Burbank well in Osage plotted in Figure 3 was retrieved from: https://waterdata.usgs.gov/monitoring-location/364337096315401/ and included in the data file as the data used is not stored on the USGS site. The well injection data used in this manuscript are kept by https://oklahoma.gov/occ/divisions/oil-gas/oil-gas-data.html under the *Arbuckle AOI Well 2012D Reported Volumes* for each year but are also included with the data file (Murray et al., 2024a). Additional well log datums were taken from 1002A and Survey reports for the wells and can be found via individual search by API or well name at https://public.occ.ok.gov/OGCDWellRecords/.

During the time period of the study, the OGS was not a USGS Advanced National Seismic System Tier 1 network and there are discrepancies between the catalogs; the OGS catalog (Walter et al., 2020) includes smaller magnitude events not available from the USGS Comprehensive Catalog https://earthquake.usgs.gov/data/comcat/. The global earthquake information used in this paper was downloaded from the USGS Comprehensive Catalog. Tidal analysis was performed using SlugTide (Nale & Brodsky, 2014), a collection of Matlab codes developed at the University of California, Santa Cruz (Allègre et al., 2016; Xue et al., 2013).

Acknowledgments
We thank Kim Hatfield of Crawley Energy & the Petroleum Alliance of Oklahoma. We thank University of Oklahoma students: M.R. McConville, J.A. Williams M.S., P.G. Perilla-Castillo. We thank reviewers Andrew Barbour, Chi-Yuen Wang, two anonymous reviewers, and AE Brandon Dugan. Allen & Hayman were partly supported by National Science Foundation award #2317726 and U.S. Department of Energy (DOE) award DE-FE0031837. This material is based upon work supported by the Department of Energy under Award Number DE-FE0032374. Initial funding came from the Oklahoma Independent Petroleum Alliance and Oklahoma Oil and Gas Association which have since merged into the Petroleum Alliance of Oklahoma.

References

Ackworth, R. I., Rau, G. C., McCallum, A. M., Anderson, M. S., & Cuthbert, M. O. (2015). Understanding connected surface-water/groundwater systems using Fourier analysis of daily and sub-daily head fluctuation. *Hydrogeology Journal*, *23*(1), 143–159. https://doi.org/10.1007/s10040-014-1182-5

Allègre, V., Brodsky, E. E., Xue, L., Nale, S. M., Parker, B. L., & Cherry, J. A. (2016). Using earth-tide induced water pressure changes to measure in situ permeability: A comparison with long-term pumping tests. *Water Resources Research*, *52*(4), 3113–3126. https://doi.org/10.1002/2015WR017346

Al-Shaieb, Z., & Lynch, M. (1993). Paleokarstic features and thermal overprints observed in some of the Arbuckle cores of Oklahoma. In *Paleokarst related hydrocarbon reservoirs*.

Al-Shaieb, Z., Puckette, J. O., Abdalla, A. A., & Ely, P. B. (1994). Megacompartment Complex in the Anadarko Basin: A completely sealed overpressured phenomenon. In *Basin compartments and seals*. American Association of Petroleum Geologists. https://doi.org/10.1306/M61588C4

Ansari, E., Bidgoli, T. S., & Hollenbach, A. (2019). Accelerated fill-up of the arbuckle group aquifer and links to U.S. Midcontinent seismicity. *Journal of Geophysical Research: Solid Earth*, *124*(3), 2670–2683. https://doi.org/10.1029/2018JB016926

Barbour, A. J. (2015). Pore pressure sensitivities to dynamic strains: Observations in active tectonic regions. *Journal of Geophysical Research: Solid Earth*, *120*(8), 5863–5883. https://doi.org/10.1002/2015JB012201

Barbour, A. J., & Beeler, N. M. (2021). Teleseismic waves reveal anisotropic poroelastic response of wastewater disposal reservoir. *Earth and Planetary Physics*, *5*(4), 1–12. https://doi.org/10.26464/epp2021034

Barbour, A. J., Norbeck, J. H., & Rubinstein, J. L. (2017). The effects of varying injection rates in Osage County, Oklahoma, on the 2016 Mw5.8 Pawnee earthquake. *Seismological Research Letters*, *88*(4), 1040–1053. https://doi.org/10.1785/0220170003

Barbour, A. J., Xue, L., Roeloffs, E., & Rubinstein, J. L. (2019). Leakage and increasing fluid pressure detected in Oklahoma's wastewater disposal reservoir. *Journal of Geophysical Research: Solid Earth*, *124*(3), 2896–2919. https://doi.org/10.1029/2019JB017327

Cardott, B. J. (2012). Thermal maturity of Woodford Shale gas and oil plays, Oklahoma, USA. *International Journal of Coal Geology*, *103*, 109–119. https://doi.org/10.1016/j.coal.2012.06.004

Crain, K., & Chang, J. (2018). *Elevation and thickness of the Ordovician Arbuckle Group in Oklahoma and surrounding states* (Open-File Report No. 2-2018). Oklahoma Geological Survey. Retrieved from http://ogs.ou.edu/docs/openfile/OF2-2018.pdf

Davies, G. R. (1979). Dolomite reservoir rocks: Processes, controls, porosity development. In *Geology of carbonate porosity*. American Association of Petroleum Geologists. https://doi.org/10.1306/CE11401C12

Dempsey, D., Kelkar, S., & Pawar, R. (2014). Passive injection: A strategy for mitigating reservoir pressurization, induced seismicity and brine migration in geologic CO_2 storage. *International Journal of Greenhouse Gas Control*, *28*, 96–113. https://doi.org/10.1016/j.ijggc.2014.06.002

Elkhoury, J. E., Brodsky, E. E., & Agnew, D. C. (2006). Seismic waves increase permeability. *Nature*, *441*(7097), 1135–1138. https://doi.org/10.1038/nature04798

Engle, M., Cozzarelli, I., & Smith, B. (2014). USGS investigations of water produced during hydrocarbon reservoir development. (Tech. Rep. No. 2014-3104). https://doi.org/10.3133/fs20143104

Franseen, E. K. (2000). A review of Arbuckle Group strata in Kansas from a sedimentologic perspective: Insights for future research from past and recent studies. *The Compass: Earth Science Journal of Sigma Gamma Epsilon*, *75*(2–3), 68–89. Retrieved from http://pubs.er.usgs.gov/publication/70022188

Franseen, E. K., & Byrnes, A. P. (2012). Arbuckle Group Platform strata in Kansas: A synthesis. In *Great American Carbonate Bank: The geology and economic resources of the Cambrian—Ordovician Sauk Megasequence of Laurentia*. American Association of Petroleum Geologists. https://doi.org/10.1306/13331528M981452

Franseen, E. K., Byrnes, A. P., Cansler, J. R., Steinhauff, D. M., Carr, T. R., & Dubois, M. K. (2004). Geological controls on variable character of Arbuckle reservoirs in Kansas: An emerging picture (Tech. Rep. No. Open File Report 2003-59). Retrieved from https://www.kgs.ku.edu/PRS/publication/2003/ofr2003-59/

Gao, X., Sato, K., & Horne, R. N. (2020). General solution for tidal behavior in confined and semiconfined aquifers considering skin and wellbore storage effects. *Water Resources Research*, *56*(6), e2020WR027195. https://doi.org/10.1029/2020WR027195

Ge, J., Nicot, J.-P., Hennings, P. H., Smye, K. M., Hosseini, S. A., Gao, R. S., & Breton, C. L. (2022). Recent water disposal and pore pressure evolution in the Delaware Mountain Group, Delaware Basin, Southeast New Mexico and West Texas, USA. *Journal of Hydrology: Regional Studies*, *40*, 101041. https://doi.org/10.1016/j.ejrh.2022.101041

Goebel, T. H. W., Rosson, Z., Brodsky, E., & Walter, J. (2019). Aftershock deficiency of induced earthquake sequences during rapid mitigation efforts in Oklahoma. *Earth and Planetary Science Letters*, *522*, 135–143. https://doi.org/10.1016/j.epsl.2019.06.036

Goebel, T. H. W., Weingarten, M., Chen, X., Haffener, J., & Brodsky, E. E. (2017). The 2016 Mw5.1 Fairview, Oklahoma earthquakes: Evidence for long-range poroelastic triggering at >40 km from fluid disposal wells. *Earth and Planetary Science Letters*, *472*, 50–61. https://doi.org/10.1016/j.epsl.2017.05.011

Guglielmi, Y., Nussbaum, C., Cappa, F., De Barros, L., Rutqvist, J., & Birkholzer, J. (2021). Field-scale fault reactivation experiments by fluid injection highlight aseismic leakage in caprock analogs: Implications for CO_2 sequestration. *International Journal of Greenhouse Gas Control*, *111*, 103471. https://doi.org/10.1016/j.ijggc.2021.103471

Hartmann, T., & Wenzel, H.-G. (1995). The HW95 tidal potential catalogue. *Geophysical Research Letters*, *22*(24), 3553–3556. https://doi.org/10.1029/95GL03324

Hawkins Jr, M. F. (1956). A note on the skin effect. *Journal of Petroleum Technology*, *8*(12), 65–66. https://doi.org/10.2118/732-G

Holubnyak, Y., Watney, W., Birdie, T., Wreath, D., Tsoflias, G., Nolte, K., et al. (2018). Lessons learned from small scale field test demonstrating CO_2 EOR and geologic storage at Wellington field in Southern Kansas. In *14th Greenhouse Gas Control Technologies Conference Melbourne 21-26 October 2018 (GHGT-14)*. https://doi.org/10.2139/ssrn.3365741

Hsieh, P. A., & Bredehoeft, J. D. (1981). A reservoir analysis of the Denver earthquakes: A case of induced seismicity. *Journal of Geophysical Research*, *86*(B2), 903–920. https://doi.org/10.1029/JB086iB02p00903

Hsieh, P. A., Bredehoeft, J. D., & Rojstaczer, S. A. (1988). Response of well aquifer systems to earth tides: Problem revisited. *Water Resources Research*, *24*(3), 468–472. https://doi.org/10.1029/WR024i003p00468

Hvorslev, M. J. (1951). *Time lag and soil permeability in ground-water observations* (Bulletin No. 36) (p. 50). Waterways Experiment Station, US Army Corps of Engineers..

Kennel, J., & Parker, B. (2023). earthtide: Parallel implementation of 'ETERNA 3.40' for prediction and analysis of Earth tides [Computer software manual]. Retrieved from https://github.com/jkennel/earthtide

Keranen, K. M., Savage, H. M., Abers, G. A., & Cochran, E. S. (2013). Potentially induced earthquakes in Oklahoma, USA: Links between wastewater injection and the 2011 Mw 5.7 earthquake sequence. *Geology*, *41*(6), 699–702. https://doi.org/10.1130/G34045.1

Keranen, K. M., & Weingarten, M. (2018). Induced seismicity. *Annual Review of Earth and Planetary Sciences*, *46*(1), 149–174. https://doi.org/10.1146/annurev-earth-082517-010054

Kerans, C. (1988). Karst-controlled reservoir heterogeneity in Ellenburger group carbonates of west Texas-1. *AAPG Bulletin*, *72*(10), 1160–1183. https://doi.org/10.1306/703C996F-1707-11D7-8645000102C1865D

King, C. Y., Azuma, S., Igarashi, G., Ohno, M., Saito, H., & Wakita, H. (1999). Earthquake-related water-level changes at 16 closely clustered wells in Tono, central Japan. *Journal of Geophysical Research*, *104*(86), 13073–13082. https://doi.org/10.1029/1999JB900080

Kolawole, F., Johnston, C., Morgan, C., Chang, J. C., Marfurt, K. J., Lockner, D. A., et al. (2019). The susceptibility of Oklahoma's basement to seismic reactivation. *Nature Geoscience*, *12*(10), 1–6. https://doi.org/10.1038/s41561-019-0440-5

Koranne, S. (2011). Hierarchical data format 5: HDF5 [Software]. In *Handbook of open source tools* (pp. 191–200). Springer. Retrieved from https://www.hdfgroup.org

Kroll, K. A., Cochran, E. S., & Murray, K. E. (2017). Properties of the Arbuckle group in Oklahoma derived from well fluid level response to the 3 September 2016 Mw 5.8 Pawnee and 7 November 2016 Mw 5.0 Cushing Earthquakes. *Seismological Research Letters*, *88*(4), 963–970. https://doi.org/10.1785/0220160228

Kurdyavtsev, S. M. (2004). Improved harmonic development of the Earth tide-generating potential. *Journal of Geodesy*, *77*(12), 829–838. https://doi.org/10.1007/3-540-27432-4_79

Langenbruch, C., Weingarten, M., & Zoback, M. D. (2018). Physics-based forecasting of man-made earthquake hazards in Oklahoma and Kansas. *Nature Communication*, *9*(1), 3946. https://doi.org/10.1038/s41467-018-06167-4

Langenbruch, C., & Zoback, M. D. (2016). How will induced seismicity in Oklahoma respond to decreased saltwater injection rates? *Science Advances*, *2*(11), e1601542. https://doi.org/10.1126/sciadv.1601542

Lawson, J. E., & Luza, K. V. (1995). *Earthquake map of Oklahoma (with explanatory text)* (OGS Geologic Map No. 35). Oklahoma Geological Survey (Scale 1:500,000). Retrieved from http://ogs.ou.edu/docs/geologicmaps/GM35M.pdf

Lemons, C., McDaid, G., Smye, K., Acevedo, J. P., Hennings, P. H., Banerji, D. A., & Scanlon, B. R. (2019). Spatiotemporal and stratigraphic trends in salt-water disposal practices of the Permian Basin, Texas and New Mexico, United States. *Environmental Geosciences*, *26*(4), 107–124. https://doi.org/10.1306/eg.06201919002

Liao, X., Wang, G., & Shi, Z. (2020). Sustained changes in well water levels following a large earthquake: Possible evidence of permeability decreases in a shallow groundwater system. *Geophysical Research Letters*, *48*(1), e2020GL090232. https://doi.org/10.1029/2020GL090232

Loucks, R. G., Mescher, P. K., & McMechan, G. A. (2004). 05). Three-dimensional architecture of a coalesced, collapsed-paleocave system in the Lower Ordovician Ellenburger Group, central Texas. *AAPG Bulletin*, *88*(5), 545–564. https://doi.org/10.1306/12220303072

Merritt, M. L. (2004). *Estimating hydraulic properties of the Floridian aquifer system by analysis of Earth-tide, ocean-tide, and barometric effects, Collier and Hendry Counties, Florida* (Water-Resources Investigation Report No. 03-4267). United States Geological Survey. https://doi.org/10.3133/wri034267

Middleton, R. S., Ogland-Hand, J. D., Chen, B., Bielicki, J. M., Ellett, K. M., Harp, D. R., & Kammer, R. M. (2020). Identifying geologic characteristics and operational decisions to meet global carbon sequestration goals. *Energy & Environmental Science*, *13*(12), 5000–5016. https://doi.org/10.1039/D0EE02488K

Morgan, B. C., & Murray, K. E. (2015). Characterizing small-scale permeability of the Arbuckle Group, Oklahoma (Tech. Rep. No. Open File Report 2-2015). Retrieved from http://www.ogs.ou.edu/pubsscanned/openfile/OF2015_2MorganMurray.pdf

Murray, K. E., Allen, B., & Hayman, N. W. (2024a). Subsurface monitoring of Arbuckle fluid pressure [Dataset]. https://doi.org/10.5281/zenodo.12706698

Murray, K. E., Allen, B., & Hayman, N. W. (2024b). Well pressure in the Arbuckle Group from 2016-2020, Oklahoma (Tech. Rep. No. Open File Report 1-2024). Retrieved from https://ou.edu/content/dam/ogs/documents/OFRs/OFR1_Well%20Pressure_2024.pdf

Murray, K. E., Brooks, C., Walter, J. I., & Ogwari, P. O. (2023). Oklahoma's coordinated response to more than a decade of elevated seismicity. In *Recent seismicity in the southern midcontinent, USA: Scientific, regulatory, and industry responses*. Geological Society of America. https://doi.org/10.1130/2023.2559(02)

Nale, S., & Brodsky, E. E. (2014). Slugtide [software]. https://github.com/eebrodsky/SlugTide/tree/main

Norbeck, J. H., & Rubinstein, J. L. (2018). Hydromechanical earthquake nucleation model forecasts onset, peak, and falling rates of induced seismicity in Oklahoma and Kansas. *Geophysical Research Letters*, *45*(7), 2963–2975. https://doi.org/10.1002/2017GL076562

Northcutt, R. A., & Campbell, J. A. (1995). Geologic provinces of Oklahoma (Open-File Report No. OF5-95). Retrieved from http://ogs.ou.edu/docs/openfile/OF5-95.pdf

Oklahoma Corporation Commission. (2016). *Initial earthquake response: Cushing 11/8/2016: Advisory 4 – Cushing*. News Release (News Release). Oklahoma Corporation Commission.

Ortiz, J. P., Person, M. A., Mozley, P. S., Evans, J. P., & Bilek, S. L. (2019). The role of fault-zone architectural elements on pore pressure propagation and induced seismicity. *Groundwater*, *57*(3), 465–478. https://doi.org/10.1111/gwat.12818

Pollyea, R. M., Chapman, M. C., Jayne, R. S., & Wu, H. (2019). High density oilfield wastewater disposal causes deeper, stronger, and more persistent earthquakes. *Nature Communications*, *10*(1), 3077. https://doi.org/10.1038/s41467-019-11029-8

Roeloffs, E. (1996). Poroelastic techniques in the study of earthquake-related hydrologic phenomena. In R. Dmowska & B. Saltzman (Eds.), *Advances in geophysics* (Vol. 37, pp. 135–197). https://doi.org/10.1016/S0065-2687(08)60270-8

Ross, R. J. J. (1976). Ordovician sedimentation in the western United States. In *The Ordovician system: Proceedings of a paleontological association Symposium: Birmingham* (pp. 73–105).

Rottman, K. (2018). *Well-log characterization of the Arbuckle in central and northern Oklahoma: Interpretation of the impact of its depositional and post-depositional history on injection induced seismicity* (Open File Report No. 21-2018). Oklahoma Geological Survey. Retrieved from https://ou.edu/content/dam/ogs/documents/data/OFR21-2018.pdf

Rottmann, K. (2018). Well-log charcterization of the Arbuckle Group in Central and Northern Oklahoma: Interpretation of the impact of its depositional and post-depositional history on injection induced seismicity (Tech. Rep. No. Open File Report 21-2018). Retrieved from https://ou.edu/content/dam/ogs/documents/data/OFR21-2018.pdf

Schultz, R. A., Heinemann, N., Horváth, B., Wickens, J., Miocic, J. M., Babarinde, O. O., et al. (2023). An overview of underground energy-related product storage and sequestration. *Geological Society, London, Special Publications*, *528*(1), 15–35. SP528-2022-160. https://doi.org/10.1144/SP528-2022-160

Skoumal, R. J., Barbour, A. J., Brudzinski, M. R., Langenkamp, T., & Kaven, J. O. (2020). Induced seismicity in the Delaware Basin, Texas. *Journal of Geophysical Research: Solid Earth*, *125*(1), e2019JB018558. https://doi.org/10.1029/2019JB018558

Smye, K. M., Ge, J., Calle, A., Morris, A., Horne, E. A., Eastwood, R. L., et al. (2024). Role of deep fluid injection in induced seismicity in the Delaware basin, west Texas and southeast New Mexico. *Geochemistry, Geophysics, Geosystems*, *25*(6), e2023GC011260. https://doi.org/10.1029/2023GC011260

Suhm, R. W. (2016). *Simpson play (including parts of the Arbuckle and Viola)* (Open File Report No. 3-2016). Oklahoma Geological Survey. Retrieved from http://ogs.ou.edu/docs/openfile/OF3-2016.pdf

Walsh, F. R., III., & Zoback, M. D. (2015). Oklahoma's recent earthquakes and saltwater disposal. *Science Advances*, *1*(5), 9. https://doi.org/10.1126/sciadv.1500195

Walter, J. I., Ogwari, P., Ferrer, F., Woelfel, I., Chang, J., Darold, A., & Holland, A. (2020). The Oklahoma geological survey statewide seismic network. *Seismological Research Letters*, *91*(2), 611–621. https://doi.org/10.1785/0220190211

Wang, C.-Y., Doan, M.-L., Xue, L., & Barbour, A. J. (2018). Tidal response of groundwater in a leaky aquifer—Application to Oklahoma. *Water Resources Research*, *54*(10), 8019–8033. https://doi.org/10.1029/2018WR022793

Wang, G., Li, P., Hao, F., Zou, H., & Yu, X. (2015). Dolomitization process and its implications for porosity development in dolostones: A case study from the Lower Triassic Feixianguan Formation, Jiannan area, Eastern Sichuan Basin, China. *Journal of Petroleum Science and Engineering*, *131*, 184–199. https://doi.org/10.1016/j.petrol.2015.04.011

White, J. A., Chiaramonte, L., Ezzedine, S., Foxall, W., Hao, Y., Ramirez, A., & McNab, W. (2014). Geomechanical behavior of the reservoir and caprock system at the In Salah CO_2 storage project. *Proceedings of the National Academy of Sciences of the United States of America*, *111*(24), 8747–8752. https://doi.org/10.1073/pnas.1316465111

Xue, L., Li, H.-B., Brodsky, E. E., Xu, Z.-Q., Kano, Y., Wang, H., et al. (2013). Continuous permeability measurements record healing inside the Wenchuan earthquake fault zone. *Science*, *340*(6140), 1555–1559. https://doi.org/10.1126/science.1237237

Yeck, W. L., Weingarten, M., Benz, H. M., McNamara, D., Bergman, E. A., Herrmann, R. B., et al. (2016). Far-field pressurization likely caused one of the largest injection induced earthquakes by reactivating a large preexisting basement fault structure. *Geophysical Research Letters*, *43*(19), 10198–10207. https://doi.org/10.1002/2016GL070861

Zhang, Y., & Huang, F. (2011). Mechanism of different coseismic water-level changes in wells with similar epicentral distances of intermediate field. *Bulletin of the Seismological Society of America*, *101*(4), 1531–1541. https://doi.org/10.1785/0120100104